Biofabrication

International Society for Biofabrication

The development of a high throughput drug-responsive model of white adipose tissue comprising adipogenic 3T3-L1 cells in a 3D matrix

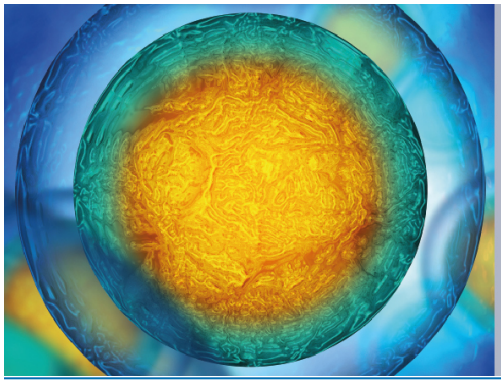

Biofabrication

OPEN ACCESS

RECEIVED
23 July 2019

REVISED
21 October 2019

ACCEPTED FOR PUBLICATION
12 November 2019

PUBLISHED
11 December 2019

PAPER

The development of a high throughput drug-responsive model of white adipose tissue comprising adipogenic 3T3-L1 cells in a 3D matrix

Alexander D Graham[1,6], Rajesh Pandey[2,6], Viktoriya S Tsancheva[1], Alessia Candeo[3], Stanley W Botchway[3], Alasdair J Allan[4], Lydia Teboul[4], Kamel Madi[5], Tahkur S Babra[1], Louisa A K Zolkiewski[2], Xuan Xue[1], Liz Bentley[2], Joan Gannon[1], Sam N Olof[1,7] and Roger D Cox[2,7]

[1] OxSyBio Ltd, Building R27, Rutherford Appleton Laboratory, Harwell Campus, Didcot, Oxfordshire, OX11 0QX, United Kingdom
[2] Medical Research Council Harwell Institute, Mammalian Genetics Unit, Harwell Campus, Oxfordshire, OX11 0RD, United Kingdom
[3] Central Laser Facility—Science & Technology Facility Council, The Research Complex at Harwell, Rutherford Appleton Laboratory, Harwell Campus, Didcot, Oxfordshire, OX11 0FA, United Kingdom
[4] Medical Research Council Harwell Institute, Mary Lyon Centre, Harwell Campus, Oxfordshire, OX11 0RD, United Kingdom
[5] 3Dmagination, Building R27, Rutherford Appleton Laboratory, Harwell Campus, Didcot, Oxfordshire, OX11 0QX, United Kingdom
[6] These authors contributed equally to this work.
[7] Authors to whom any correspondence should be addressed.

E-mail: sam.nicholas.olof@gmail.com **and** r.cox@har.mrc.ac.uk

Keywords: adipose, spheroids, 3D culture

Supplementary material for this article is available online

Abstract

Adipose models have been applied to mechanistic studies of metabolic diseases (such as diabetes) and the subsequent discovery of new therapeutics. However, typical models are either insufficiently complex (2D cell cultures) or expensive and labor intensive (mice/*in vivo*). To bridge the gap between these models and in order to better inform pre-clinical studies we have developed a drug-responsive 3D model of white adipose tissue (WAT). Here, spheroids (680 $\pm$ 60 μm) comprising adipogenic 3T3-L1 cells encapsulated in 3D matrix were fabricated manually on a 96 well scale. Spheroids were highly characterised for lipid morphology, selected metabolite and adipokine secretion, and gene expression; displaying significant upregulation of certain adipogenic-specific genes compared with a 2D model. Furthermore, induction of lipolysis and promotion of lipogenesis in spheroids could be triggered by exposure to 8-br-cAMP and oleic-acid respectively. Metabolic and high content imaging data of spheroids exposed to an adipose-targeting drug, rosiglitazone, resulted in dose-responsive behavior. Thus, our 3D WAT model has potential as a powerful scalable tool for compound screening and for investigating adipose biology.

Introduction

It is estimated by the International Diabetes Federation (IDF) that in 2017, 425 million adults worldwide had diabetes, approximately 90% of them having type 2 diabetes ([1] (https://diabetesatlas.org/resources/2017-atlas.html)). Diabetes is a major cause of blindness, kidney failure, cardiovascular disease (CVD), stroke and lower limb amputation. Obesity and alterations in fat distribution (measured as waist-hip-ratio adjusted for Body Mass Index (WHRadjBMI)) are significant risk factors for both type 2 diabetes and CVD [2–4]. In 2015 CVD prevalence was approximately 422 million cases globally [5]. The burden of these diseases is likely to increase as the global obesity prevalence is predicted to reach 18% in men and 21% in women by 2025 [1, 6]. Obesity is also associated with a range of other conditions including non-alcoholic fatty liver disease (NAFLD), cirrhosis and cancer. Thus, given the demonstrable global health challenge, there is a critical need to better understand the role of adiposity and fat distribution in determining disease risk. In addition to environmental factors such as diet and exercise, obesity and alterations in fat distribution have a strong heritable component and indeed 500 adiposity trait associations

and 463 WHRadjBMI signals have been mapped in human genome wide association studies [7, 8]. Understanding the mechanisms underlying these traits will allow the development of new therapeutic approaches to mitigate the obesity epidemic and its adverse effects on health.

Translating information from human population genetic studies into biological mechanisms and tools for precision medicine requires application of a broad set of strategies including genetic fine mapping in different human populations, genomic and epigenomic studies, physiological experiments on volunteers of known genotype, and mechanistic studies in animal and cellular models (reviewed [9]). A common approach for the cellular studies, a key part of these strategies, is the use of simple *in vitro* two-dimensional (2D) models comprising cell lines and primary cells. These are valuable models essential for understanding adipocyte behaviour and differentiation, and for compound screening [10–12]. However, monolayer models, whilst fast and inexpensive lack the complexity of adult *in vivo* tissue in terms of cell types, cellular interactions and morphology. Hence, animals are commonly employed as translational models to study specific organs, such as adipose, and the organismal response to compounds, however, this research is expensive and labour intensive. Therefore, a model that bridges the gap between 2D cellular discovery studies and *in vivo* pre-clinical models, such as the mouse, in an inexpensive manner would be desirable. Such a model could facilitate mechanistic work at scale before transitioning to *in vivo* models, as well as allowing high throughput screening of compounds for more diverse endpoints. A three-dimensional (3D) cell culture system could help bridge this gap by more accurately representing the complexity and functional output of adipose physiology. Specifically, 2D cultures may be exceeded by 3D cell culture systems which enhance adipocyte maturation through cell-to-cell interactions in a 3D environment and extracellular matrix development (ECM development). 3D models could also allow for the addition of vasculature and immune components (i.e. macrophages), acting as representative mini-adipose organ structures.

To date, several routes to the fabrication of 3D adipose cultures have been described. White adipose tissue (WAT) has been modelled by adipose spheroids [13–17], i.e. 3D colonies of adipocytes contained within sphere-like geometries. Uptake of this type of model has become more commonplace due to the 3D morphological complexity of spheroids and their compatibility with multi-well microtitre plates. In one process, scaffold-free hanging drop spheroids of murine and human cells from various sources have been shown to differentiate and secrete adiponectin as well as being suitable for high throughput screening platforms [13]. Human adipose derived stem cells have also been incorporated into hanging drop cultures as well as conventional spheroids and successfully differentiated, raising the possibility of using human primary cells or induced pluripotent stem cells (iPSCs) in such systems for screening [14, 15]. Further, as adipose tissue is highly vascularized, vascularized adipose spheroids from human stromal vascular fraction cell preparations have been described and the endothelial cell vessels shown to connect to recipient circulatory systems when transplanted into mice [16]. Similarly, a polylysine-based magnetic nanoparticle system to levitate 3D droplet cultures of 3T3-L1 cells has been shown to differentiate and form vascular like structures with the addition of endothelial cells [17]. 3D adipose models may be fabricated by alternative routes, such as the bioprinting of cellularised matrices [18, 19], the seeding of cm-scale scaffolds / matrices [20, 21], the generation of adipose fibres using cell fibre technologies [22] and the maturation of 3D adipocyte colonies in perfusable vessels such as bioreactors [23, 24] and microfluidic chips [25, 26]. While some of these non-spheroid methods have the potential to offer higher complexity adipose models in the future, they are currently less compatible with high-throughput screening platforms than spheroid techniques. In addition to modelling adipose tissues, 3D adipose cultures have also been developed for wound healing [27] and regenerative medicine [18, 28, 29] applications by incorporating self-renewing adipose derived stem cells. These studies demonstrate the feasibility of developing differentiating 3D adipose cell cultures and of humanising and/or adding to their complexity. More complex 3D culture systems may be used to investigate cell interactions and paracrine effects that are important *in vivo*.

To be suitable for therapeutic studies, any 3D adipose model would invariably have to reproduce and exceed the complexity of established 2D culture. The model would also have to be compatible with high throughput formats for compound screening and display a range of measurable functional outputs e.g. hormone secretion, lipogenesis, lipolysis and glycerol secretion. To address this, we have developed and characterised a synthetic 3D model of WAT, focusing on designing a model that not only captures adipose biology but is simple to create, robust and responsive to adipose-targeting drugs. To build our 3D WAT model we have adapted workflows developed for the 3D bioprinting of generic cellularised constructs [30]. However, in contrast to methods developed exclusively for 3D printing, here we present a user-friendly, inexpensive method to produce spheroids, from 3T3-L1 cells encapsulated in a hydrogel matrix. The 3D WAT model displayed synthesis of lipid stores and expression of adipogenic markers, which predominantly exceeded 2D adipose controls, and retained an active and drug-responsive lipid metabolism. Furthermore, to enable high throughput workflows such as compound screening, we have reproducibly fabricated and cultured our 3D WAT model in a 96-well plate format. This has allowed us to

employ automated methodologies such as robotic liquid handling and novel high-content imaging assays for monitoring the functional outputs of the 3D WAT model.

Methods

Culture of pre-adipocytes

The mouse-derived 3T3-L1 (ATCC, CL-173) was cultured using DMEM containing high glucose, GlutaMAX™ and pyruvate (Gibco, Cat. 31966) supplemented with 10% v/v new born calf serum (NBCS, Gibco, Cat. 26010-074) at 37 °C with 5% CO_2. TrypLE express 1 × (Gibco, Cat. 12605-010) was used to dissociate the cells. During cell expansion, cells were sub-cultured at approximately 70% confluency. Only cells between passage number 6 and 15, and with ⩾90% viability, have been used for experiments. Prior to addition to the matrix, the total cell number and viability of harvested cells were determined using an automated cell counter (Countess II, Thermo Fisher Scientific).

Hydrogel-based matrix preparation

The hydrogel-based matrix consisted of an 8:1 v:v mixture of ultra-low gelling temperature agarose (ULGT-agarose) solution to fluorenyl-methyloxycarbonyl (Fmoc)-dipeptide solution. To this working solution collagen suspended in 1 × PBS (phosphate buffered saline, Sigma Aldrich or Gibco) was added, in a process described below. Typically, ULGT agarose (14 mg ml^{-1}, Sigma-Aldrich, Cat. A5030) dissolved in DMEM (Gibco, Cat. 31966) was heated to 65 °C. Added to this was a 1:1 v:v mixture of 10 mM Fmoc-diphenylalanine (Fmoc-FF, pH 8.5, Bachem) and 10 mM Fmoc-isoleucine-glycine (Fmoc-IG, pH 9.5 to 10.5, Bachem) in deionised water (supplementary methods). For sterility, the solution was sterilized by UV irradiation (15 min, 365 nm) at 4.5 cm from an UV LED (Eclipse-M365L2-C5, Nikon) controlled by an LED driver (LEDD1B, Thorlabs) set to half power. The sterile solution was then left to stand (∼5 min) at 50 °C prior to ice cold collagen addition. The ULGT-agarose/Fmoc-dipeptide solution was supplemented with type I collagen (bovine; Life Technologies) as a 3 mg ml^{-1} solution (supplementary methods) and diluted to 90% volume with additional 1 × PBS to give a solution of 11.2 mg ml^{-1} ULGT-agarose, 0.5 mM Fmoc-IG, 0.5 mM Fmoc-FF and 15 μg ml^{-1} type I collagen. The matrix was sonicated immediately prior to cell addition (⩾5 min, 40 °C, 40 kHz) in a ultrasonic bath (2.75 L S-Series, Fisherbrand™). The cells were harvested and centrifuged (4 min, 300 × g) to give a pellet, which was resuspended in matrix (200 μl) at a cell density of 40 × 10^6 cells ml^{-1}. All matrix solutions were used on the day they were made.

Spheroid fabrication

Droplets (170 ± 40 nl) of matrix suspended with cells were dispensed manually by pipette (0.2-2.0 μl models) into an oil mixture held within a custom container comprising a 6 × 6 array of 2.0 mm diameter wells by 1.5 mm depth. The oil consisted of a 35:65 v:v mixture of undecane (Sigma-Aldrich, Cat. U407) to silicone oil AR20 (Sigma-Aldrich, Cat. 10836) supplemented with 1.2 mM 1,2-diphytanoyl-sn-glycero-3-phosphocholine (DPhPC, Avanti Polar Lipids, Cat. 850356 P). Due to the viscosity of the solution, dispensing involved loading the pipette with 2 μl of matrix solution and gently pushing out ∼150 nl into the oil as assessed by eye using a stereomicroscope. A droplet could then be formed by raising the pipette tip out of the oil. The remaining solution would be used to fabricate subsequent droplets in a similar manner. Once formed, the cellularised liquid droplets were gelled by allowing to stand at 4 °C for 25 min. Cellularised droplets were transferred into 96-well U-bottom plates with cell repellent surfaces (Greiner; Cat. 650970) containing culture medium to give one to three spheroids per well. This was performed by aspirating one to three spheroids into a truncated pipette tip (20 μl) and dispensing them into the desired well which comprised of 50 μl of transfer oil (a 3:1 v:v mixture of hexadecane (Sigma-Aldrich, Cat. 296317) to mineral oil (Sigma-Aldrich, Cat. M3516) layered above 120 μl of 3D culture medium. The plate was centrifuged (300 × g, 1 min) to ensure total phase transfer. After the cellularised droplet moved into the culture medium, the upper oil phase was removed by pipette aspiration and additional culture medium (80 μl) was added by pipette. Aqueous-bound cellularised droplets i.e. spheroids were moved to the incubator (37 °C and 5% CO_2) for culture and cells would typically condense within 24 h as assessed by microscope.

Adipogenic differentiation of spheroids and control 2D cells

Spheroids were differentiated by following a strict culture regime. Cells proliferated for the initial 48 h (day 0 to day 2) in standard culture media (DMEM, Gibco, Cat. 31966), supplemented with 10% v/v NBCS and 1% v/v penicillin-streptomycin mixture (Pen-Strep, 10 000 U ml^{-1}, Gibco, Cat. 15140-122). On day 2 of the spheroid culture, adipogenic differentiation was induced using differentiation medium (DMEM, Gibco, Cat. 31966) with 10% v/v foetal bovine serum (FBS, Gibco, Cat. 10270-106 and 1% v/v Pen-strep) containing an adipogenic cocktail (0.1% v/v IBMX (3-isobutyl-1-methylxanthine, 0.5 M), 0.05% v/v dexamethasone (2 mM) and 0.05% v/v insulin (1.72 mM/10 mg ml^{-1}). After culture in differentiation medium for 4 d (day 2 to day 6), the spheroids were cultured using maintenance medium ((DMEM, 10% v/v FBS, 1% v/v Pen-Strep and 0.05% v/v insulin (1.72 mM/10 mg ml^{-1}) till day 30 (day 28

of differentiation conditions). The control set of non-differentiated spheroids were cultured using the standard culture media from day 0 to day 30. The media for all the spheroids were changed every 2–3 d and the culture volume was 200 μl of medium. The process for changing medium involved repeatedly (2–3 times) aspirating the upper ~120 μl solution of each well and adding fresh medium (~120 μl) either manually or using the liquid handling robot (Assist Plus, Integra Biosciences). The 2D cells were seeded at 6,000 cells per well in 96-well plates (Greiner, Cat. 655098). Differentiation of 2D cells was performed in the same manner as spheroids except, the initial proliferation step was over 3 d instead of 2 d.

High content imaging and image analysis

A multimode plate reader and high content imager (Cytation 1, BioTek), was used for brightfield and fluorescence imaging of all samples. Spheroids (in 96-well plates) and 2D cells grown on coverslips (in 6-well plates) were assessed for spheroid size, cell aggregate size, cell viability and lipid content. Software (Gen 5, BioTek) was used for image acquisition, processing and analysis. Each characterisation method employed optimised image acquisition settings to typically record a standardised *z*-stack image set with the signal intensity of pixels falling within the dynamic range of the camera. Image stacks were processed as maximum intensity projections, which were then analysed using Gen5's 'cellular analysis' function. This enabled the counting of the area within a region of interest as defined by the analysis function settings which included threshold limits for pixel intensity and object size. This function was employed to quantify spheroid diameters (from phase contrasted brightfield images). Here it was assumed the images represented a circular cross-section of the spheroid at its centre, with the diameter of the circle matching that of the spheroid. Volume could then be calculated using the diameter value by assuming a spherical geometry of the spheroid. Cell viability was estimated from fluorescence images, using the measurements of the areas of live cell signal (calcein-AM) and dead cell signal (propidium iodide). Finally, relative lipid signal was determined by normalising lipid signal (BODIPY493/503) to nuclei signal (Hoechst 33342) as a percentage value. While high-intensity lipid was determined as a percentage by comparing the area of lipid signal above the intensity of 15 000 per pixel to the total area of all lipid signal. All other image analysis unless otherwise stated was performed manually using ImageJ, specifically by fitting circular regions of interest to lipid droplet organelles or the entire spheroid cross-section.

Proliferation assay

Proliferation assays were performed using an alamarBlue® cell viability assay (Thermo Fisher Scientific, Cat. DAL1025) on 2D cells and spheroids on day 1, 2, 3 and 4 of culture. On the day of experiment, alamarBlue reagent (resazurin) was mixed at a ratio of 1:10 v:v with the sample's culture medium and the sample was left to incubate (37 °C, 5% CO_2, 4 h). Fluorescence was quantified using a multimode microplate reader (Varioskan Flash, Thermo Fisher Scientific). Fluorescence excitation wavelength of 540–570 nm (peak excitation is 570 nm) and emission at 580–610 nm (peak emission is 585 nm) were used. A standard curve for resorufin fluorescence versus cell number was created for the proliferation assay from a cell titration assay.

Live/dead assay

Live/dead staining of spheroids either exposed to adipogenesis cocktail or culture without (control) was performed on days 0, 7, 14 and 28 of adipogenesis. Staining applied include calcein-AM (CAM) dye (Cayman Chemical, CAY14948) in conjunction with propidium iodide (PI) dye (Sigma-Aldrich, Cat. P4170). Stock dye solutions, CAM (5 mM in DMSO) and PI (5 mM in DMSO) were each added at a 1000-fold dilution to culture medium, to give a 5 μM working dye solution. Spheroids for the live/dead assay were transferred to a new 96-well plate with 20 μl of medium, and then dye solution was added (150 μl). The samples were left to stain by standing (in the dark) in the incubator (37 °C, 5% CO_2, 30 min). Samples were washed once with culture-medium and 150 μl of fresh media was added. Before imaging, 50 μl of mineral oil was added on top of the wells for imaging efficiency. For each condition, we have used $N = 5$ samples. Imaging was done using a multi-mode reader (Cytation 1, BioTek). Imaging settings were kept consistent across all experiments

Lipid morphology

Lipid morphology was investigated by fluorescence imaging of 2D cells and spheroids fixed at either day 0, 7, 14 and 28 of adipogenesis ($N = 4$ for 3D and $N = 3$ for 2D per time point). Fixation was by exposing samples to 4% w/v paraformaldehyde (200 μl) for 1 h. Samples were stained in batch for a combination of either lipid droplets (BODIPY 493/503, Thermo Fisher Scientific, Cat. D3922), nuclei (NucBlue™, Thermo Fisher Scientific, Cat. H3570), cell membrane proteins (MemBrite™ Fix 640/660, Biotium, Cat. 30098) or perilipin (PLIN1, Immunocytochemistry (ICC), Abcam, Cat. ab61682). All staining was performed consecutively, with 1 × PBS wash steps applied before and after specific dye staining. MemBrite™ 640/660 staining was conducted prior to fixation following the manufacturer's instructions (supplementary methods). PLIN1 ICC was performed after fixation with primary antibody: goat polyclonal to perilipin A-carboxyterminal end (Abcam, Cat. ab61682) and secondary antibody: donkey anti-goat conjugated with Alexa Fluor 647 (Abcam, Cat.

ab150135) (supplementary methods). BODIPY 493/503 and NucBlue staining was performed on fixed samples (after ICC, if PLIN1 stained) by dye exposure at 3.8 μM and 2 drops per ml concentrations respectively over 30 min (2D) or 1 h (spheroids) (supplementary methods). Samples were stored in 1 × PBS solution at 4 °C until characterisation. Imaging was by either, confocal fluorescence microscopy (LSM 700, Zeiss), light sheet fluorescence microscopy (LSFM, TCS SP8 DLS (digital light sheet), Leica) or high content imager (Cytation 1, BioTek) by applying consistent imaging setting.

Amira-avizo analysis

The image processing was performed using Thermo Scientific Amira-Avizo 9.5 software. The 3D dataset were filtered using a non-local means algorithm to reduce noise (denoise) the images while preserving the boundaries between the lipid droplets within the spheroid cells. The nuclei and lipid droplets were segmented using an interactive thresholding, which enabled computing of their respective volumes for each time point. For an image set of a day 14 of AC exposure spheroid, a few selected cells were segmented using a gradient-based watershed algorithm and used to mask the intracellular lipid droplets. A distance transform watershed algorithm was applied to separate overlapping lipid droplets. All the droplets were individually labelled and a label analysis was performed to compute their volumes. The lipid droplets were finally sieved in five regions and visualised in 3D. These values are then ranked to construct the volume distribution with a class interval size of 0.2 μm^3.

Histology

Spheroid samples were coated with tissue marking dye (Shandon™, Thermo Fisher Scientific, Cat. 3120126) with care taken not to damage the spheroid's surface. The spheroids were then sandwiched between two layers of Histogel™ (Thermo Fisher Scientific, Cat. HG-4000-012) using a custom-made PMMA mould and processed using standard tissue processing method. Samples were then paraffin-embedded and sectioned at 3 μm thickness using a standard microtome. Slides were stained with haematoxylin and eosin and imaged using a DMi8 widefield fluorescence microscope (Leica Microsystems) at ×20 and ×40 magnification. Further details can be found in the supplementary methods.

Metabolite and adipokine profiling

The extracellularly released metabolite and adipokine profiling was performed for glycerol, free fatty acids (FFAs), adiponectin and leptin. An Chemistry Analyzer (AU680, Beckman Coulter) was used to measure levels of glycerol (Randox reagents, Cat. GY105) and FFAs (enzymatic assay from Alpha Labs NEFA-HR(2) reagent 1 (Cat. 434-91795) and NEFA-HR(2) reagent 2 (Cat. 436-91995)). A Microplate Spectrophotometer (Epoch, BioTek) was used to measure leptin and adiponectin using a Leptin Mouse ELISA Assay kit (Invitrogen, Cat. KMC2281) and an Adiponectin Mouse ELISA kit (Invitrogen, Cat. KMP0041) respectively. For all the metabolites, 100 μl of culture medium was isolated after incubation and was used undiluted, except for the adiponectin assay where 1:50 dilution of culture medium was used. 2D and spheroid samples to be lysed for measuring concentrations of leptin and adiponectin were washed twice with 1 × PBS after removal of the culture medium, with spheroids frozen (−80 °C) ahead of lysing. To lyse the samples, 20 μl of Mammalian Protein Extraction Reagent (M-PER, Thermo Fisher Scientific, Cat. 78501.) was added to each samples and pipette-mixed 10 times for spheroids samples only. It was followed by incubation on ice for 30 min with intermittent gentle mixing for spheroids or constant gentle shaking for 2D samples. The resultant cell lysates were frozen (−80 °C) prior to being characterised using with the assay kits mentioned above. The incubation time of the medium was either 48 h (initial characterisation) or $\leqslant$24 h (lipolysis assay), with the medium conditioned, i.e. exchanged for fresh medium, prior to incubation. Metabolite secretion levels were normalised relative to cell numbers when comparing 2D and spheroid samples (supplementary discussion). Specifically, the concentration of metabolites in the culture media was subtracted from each of the readings for 2D and spheroid samples.

RNA isolation and cDNA synthesis

Spheroids were washed with 1 × PBS once, harvested, frozen on dry ice and stored at −80 °C on day 0, 3, 7, 10 and 14 of adipogenesis. For RNA isolation, the spheroids were thawed before being homogenized in 300 μl of phenol and guanidine isothiocyanate solution (TRIzol reagent, Thermo Fisher Scientific, Cat. 15596026) and the RNA was isolated using single cell RNA purification kit (Norgen BioTek, Cat. 51800). RNA isolation was conducted the same for 2D cells, except homogenising in phenol was performed prior to freezing. The quality and quantity of the RNA was measured using an Agilent RNA 6000 Pico kit (Cat. 5067-1513) on a Bioanalyzer (Agilent 2100). The cDNA was made using SuperScript III reverse transcriptase (Thermo Fisher Scientific, Cat. 18080044) along with random primers, deoxyribonucleotide triphosphates (dNTPs) mix, first strand buffer and dithiothreitol (DTT). cDNA was synthesised from the total RNA in 2-steps. First, RNA (10 ng) in nuclease-free water (12 μl) containing 200 ng μl^{-1} random primers (1 μl) and 10 mM dNTP mix (1 μl) was incubated (65 °C, 5 min), then chilled on ice (2 min) followed by brief centrifugation (3000 rpm for 1 min). To this solution, 5 × first strand buffer (4 μl), 0.1 M DTT (1 μl) and 200 U μl^{-1} superscript III reverse

transcriptase (1 μl) was added and incubated at 25 °C (5 min), followed by 50 °C (60 min) and 70 °C (15 min). Every reaction had a no reverse transcriptase control and a no template control. All the cDNA samples were quantified using a NanoDrop™ and normalized to 10 ng μl^{-1} concentration.

Droplet digital PCR (ddPCR)—preamplification assays

cDNA from spheroids or 2D cultures were quantified using a spectrophotometer and normalised to 10 ng μl^{-1}. Prior to ddPCR analysis, each sample was pre-amplified using the SsoAdvanced PreAmp Supermix kit (Bio-Rad, Cat. 172-5160) according to the manufacturer's instructions. In brief, 5 μl of Taqman assays for eight adipogenic marker genes and one housekeeping gene were pooled and made up to 500 μl with nuclease-free water to make a preamplification assay pool. Each reaction (50 μl) contains 25 μl SsoAdvanced PreAmp Supermix (2×), 12.5 μl preamplification assay pool, 2 μl cDNA sample and 10.5 μl nuclease-free water. The preamplification master mix was transferred to a 96-well semi-skirted plate (Eppendorf AG, Cat. 30128613) and the samples were amplified on a thermal cycler (T100, Bio-Rad) using the following protocol: 95 °C for 3 min, followed by 12 cycles of 95 °C for 15 s and 58 °C for 4 min, hold at 4 °C. The amplified samples were diluted 1:10 v:v and 2 μl of this was used for all ddPCR experiments.

ddPCR reactions

All reactions were performed in duplex, with a single adipogenic marker gene amplified in parallel with a reference gene assay (*Canx*), as an absolute quantification experiment on the ddPCR system (QX200, Bio-Rad). Reaction mixtures (22 μl) contained 2 μl pre-amplified DNA, 2 × ddPCR supermix for probes (no dUTP) (Bio-Rad, Cat. 1863024), 225 nM of each primer (two primers used per assay) and 50 nM of each probe (reference gene *Canx* labelled with VIC and an adipogenic marker gene labelled with FAM, see supplementary discussion). Reaction mixes made up to 22 μl with nuclease-free water were loaded in plate format into the ddPCR system (QX200 AutoDG, Bio-Rad) and droplets generated as per the manufacturer's instructions. Once complete, the oil/reagent emulsion was amplified on a thermal cycler (T100, Bio-Rad) using the following protocol: 95 °C for 10 min, followed by 40 cycles of 94 °C for 30 s and 58 °C for 1 min, with a final step of 98 °C for 10 min. The plate containing the droplet amplicons was subsequently loaded into the droplet reader (QX200, Bio-Rad) and an absolute quantification assay run. Standard reagents and consumables for the ddPCR system were supplied by Bio-Rad.

Analysis of ddPCR data

The droplet reader (QX200, Bio-Rad) recorded the number of accepted droplets for each sample. Accepted droplets in which fluorescence was detected (positive droplets) by either one or both channels and accepted droplets in which no fluorescence was detected (negative droplets) were recorded separately. A minimum of 10 000 accepted droplets per sample were used for analysis. Absolute quantification was calculated employing the manufacturers software (Quantasoft analysis pro software, Bio-Rad) by applying Poisson statistics to the fraction of end-point positive reactions. Data was exported for further analysis wherein transcript levels of each adipogenic marker gene was normalized to the reference gene (*Canx*). Data plotting and statistical significance was carried out using GraphPad.

qPCR

We identified specific housekeeping gene for our study from a panel of 12 housekeeping genes, using mouse geNorm kit (Primer Design, Cat. ge-DD-12) and representative set of samples (i.e. differentiated and non-differentiated 2D samples on day 0, 3, 7, 10 and 14 of AC exposure for). We used an ABI PCR System (7500 Fast Real-Time, Applied Biosystems) for this qPCR. The data showed calnexin (*Canx)* as appropriate housekeeping gene with higher and non-variable expression during adipogenic differentiation.

cAMP and Forskolin lipolysis assay

A cAMP mediated lipolysis assay was performed on spheroids (day 12) exposed to either 8-Br-cAMP (Sigma-Aldrich, Cat. B7880) or forskolin (Sigma-Aldrich, Cat. F3917). 8-Br-cAMP was prepared as a 100 mM stock solution in 1 × PBS and was exposed to spheroids at 1 and 2 mM. While Forskolin was prepared as a 10 mM stock solution in ethanol and was exposed to spheroids at 10 and 20 μM. Controls were also run for the absence of the lipolysis inducing reagents (with ethanol added for the forskolin control instead). At 0, 4, 24 and 48 h of exposure (8-Br-cAMP) or 0, 24 and 48 h (forskolin) of exposure, medium (100 μl per sample) was taken for metabolite profiling of glycerol and FFAs (see *Metabolite and Adipokine Profiling* experimental). During the reagent exposure, no insulin was present in the culture medium and all media that was removed for analysis was replaced with freshly dosed medium.

Oleic acid feeding assay

FFA feeding of spheroids (day 7) was performed by culturing samples with either 2.5 mM oleic acid (OA), 2.5 mM oleic acid-cyclodextrin (OA-CD) complex or without oleic acid (with equivalent ethanol quantities) as a control. Working solutions of FFAs were prepared by adding either stock 1.77 M OA (Sigma-Aldrich, Cat. O1383) in ethanol or 50 mg ml^{-1} OA-CD (Sigma

Aldrich, Cat. O1257) in deionised water to culture media warmed to 37 °C. These solutions were sonicated (40 kHz; 20 min) and then UV sterilised. The extent of lipid storage was assessed at 0, 48 and 120 h of oleic acid feeding. At each time-point, spheroids were fixed with 4% w/v PFA and labelled with BODIPY 493/503 (lipid) and Hoechst 33342 (nuclei) for image acquisition using a high content imager (Cytation 1, BioTek). The fluorescence micrographs were analysed by software (Gen5, BioTek) for relative lipid signal (i.e. lipid signal normalised to nuclei signal) and the proportion of lipid droplets at high-intensity (see *High Content Imaging & Analysis* experimental). During the assay period, the spheroids were cultured using a liquid handling robot (Assist Plus, Integra Biosciences) with maintenance media supplemented with insulin (0.86 μM).

Drug-responsive assay (Rosiglitazone)

A drug responsive assay was performed on spheroids ($N = 96$) by culturing them with standard adipogenic cocktail supplemented with rosiglitazone on days 2 to 6, after which standard maintenance medium was applied. Rosiglitazone (Sigma-Aldrich, Cat. R2408) was dissolved in ethanol for stock solution of 2.798 mmol l^{-1}. Rosiglitazone was then added to spheroids across a 96-well plate as a serial dilution in culture medium, with the final concentrations separated per column ranging from 12.5 μM to 12 pM. The final column of the plate held a no rosiglitazone control (ethanol added in place of rosiglitazone). At 2, 6, and 9 d of culture, medium (100 μl per sample) was taken for metabolite profiling of glycerol (see *Metabolite & Adipokine Profiling* experimental). Day 9 spheroids were fixed with 4% w/v PFA and labelled with BODIPY 493/503 (lipid) and Hoechst 33342 (nuclei) for image acquisition using a high content imager (Cytation 1, BioTek). The fluorescence micrographs were analysed by software (Gen5, BioTek) for lipid and nuclei signal (see *High Content Imaging & Analysis* experimental). We used $N = 8$ replicates for each of the conditions (except for rosiglitazone conc. of 12 pM, where a sample was lost ($N = 7$). All the media exchanges, fixation and labelling of the spheroids was performed using a liquid handling robot (Assist Plus, Integra Biosciences).

Statistics and presentation of data

Quantitative data was plotted and analysed using statistical analysis software (Prism8, GraphPad). Significance of the data was determined using two-way ANalysis Of VAriance (ANOVA, repeated measures), data not conforming to the assumptions of parametric statistical tests were transformed by square root or log10. D'Agostino and Pearson test was performed for normality. Experiments selected for significance calculations, had either $N = 3$, $N = 5$ or $N = 8$ biological replicates for each conditions, the precise number of replicates for each experiment is stated in the figure legends and the main text.

Results

In a previous report we described biofabrication methods for the 3D bioprinting of high-resolution patterned cellular constructs, which after culture, displayed tissue-like properties e.g. cartilage-like structures from printed mesenchymal stem cells [30]. Adapting this methodology, we have designed a cell-laden hydrogel-based matrix or 'bioink' (by selecting cell, hydrogel constituents and culture media components) that can be processed by hand, bioprinter or liquid handler to produce simple, monocellular 3D adipose spheroids.

Fabrication of 3T3-L1 spheroids

3T3-L1 cells were selected as a well characterized mouse pre-adipocyte cell line. They can be efficiently differentiated into mature adipocytes by treatment with insulin, dexamethasone and 3-isobutyl-1-methylxanthine (IBMX), triggering two waves of proadipogenic transcription factor activation and stimulating adipocyte gene expression [11].

In this study, 3T3-L1 cells were mixed at 40 × 10^6 ml^{-1} with a hydrogel-based matrix prior to fabrication. The key matrix components comprised of various hydrogelators, ultra-low gelling temperature (ULGT)-agarose, fluorenyl-methyloxycarbonyl (Fmoc)-dipeptides and type I collagen, i.e. a similar matrix formulation as used in the previous cell-printing work to form cartilage-like constructs [30]. The core constituent, ULGT-agarose, a linear polysaccharide, was previously selected for its compatibility with droplet-in-oil biofabrication workflows [30]. Its ability to be gelled thermally at 4 °C enabled ULGT-agarose based matrices to be dispensed as a liquid at ambient temperature and then solidified by cooling for a short duration ($\geqslant$20 min). In addition, agarose is cyto-compatible, porous and can be blended with additional bioactive components [31]. Fmoc-dipeptides were included to enhance the stability of pre-gelled printed constructs and have previously been used as scaffolds in 3D cell cultures [32]. While type I collagen, a fibrillar protein found in the extracellular matrix of most connective tissues, was blended in at low concentration. This provided biological cues in the matrix to promote cellular proliferation and tissue development; mammalian cells can adhere to type I collagen fibrils through collagen receptor integrin $\alpha2\beta2$ [33]. Type I collagen is commonly used for tissue engineering and is commercially available as a coating or scaffold for 2D and 3D cell culture respectively. The inclusion of these matrix elements, while in part artificial, has enabled the rapid processing of cells and was shown to minimally impact upon the cellular development of various models [30].

To assess the mechanical properties of the hydrogel-based matrix, rheological analysis was carried out. The shear modulus was determined for the full matrix, and in addition, how the incorporated components affect the strength of the material was also investigated (figure S1, supplementary methods and discussion are available online at stacks.iop.org/BF/12/015018/mmedia). A weak shear modulus of 44 Pa was recorded for the base mixture (ULGT-agarose). Incorporating Fmoc-dipeptides and type I collagen strengthened the hydrogel mixture to 118 Pa. This stiffness is slightly higher than that of Matrigel™ (34 Pa [34]), a gelatinous protein mixture secreted by mouse sarcoma cells, that is commonly used in organoid fabrication [35]. In comparison, adipose tissue has a stiffness of ∼1 kPa (young's modulus recorded at low strain [36]), which is higher than the matrix utilised, yet, the stiffness may increase to physiological levels during the culture and adipogenesis of suspended cells.

The cell-laden hydrogel-based matrix was dispensed manually as droplets by a micropipette into custom micro-machined well arrays (figure S2) before being transferred, post gelation, into the 96 well-plate for culture (figures 1(a)–(c) and S3). By dispensing cell-laden matrix as a liquid into oil, a sub-millimeter sized spherical droplet of matrix will form due to oil-aqueous repulsive forces. Counteracting material flattening or loss of z-resolution, which can occur when liquid hydrogels are dispensed in air onto a surface, resulting in wetting of and spreading across the surface. The size of the unmatured spheroids immediately after transfer was 680 ± 60 μm ($\overline{w}$ ± $S.D.$, $N = 96$) as measured from images recorded using a high-content imager (Cytation 1, BioTek) by area in an automated manner (Gen5 software, figures 1(d) and S4) and by manually fitting circular regions of interest (ImageJ software, figure 1(e)). The average volume of the spheroid equates to 170 ± 40 nl ($\overline{V}$ ± S.D., $N = 96$), assuming the spheroid is spherical, and contains an average of 6600 ± 1600 cells ($\overline{N}_{cell}$ ± S.D., $N = 96$).

Culture for the most part was performed using automated liquid handling robotics but could also be performed manually. Spheroids were either cultured in isolation (singlet) for image-based characterisation or as a group of three (triplet). The triplet ensured sufficient cells were present for accurate characterisation for targeted metabolites, adipokines and genetic investigations. To induce adipogenesis in the 3T3-L1 cells, the cells were initially allowed to proliferate for two days, after which adipogenesis inducing factors were introduced (figure 1(c)). A proliferation assay on triplet spheroids ($N = 5$ per condition) exposed to adipogenic cocktail (AC (insulin, IBMX and dexamethasone)) showed an increase in cell numbers from 18 000 ± 11 000 on day 1 to 42 000 ± 9000 on day 2 ($\overline{N}_{cell}$ ± S.D.) i.e. the start of adipogenesis inducing factor exposure (figure 1(f)). After adipogenic growth factor introduction, the cell number remained roughly constant for the subsequent 48 h of exposure. Comparably, a control triplet spheroid cultured without adipogenic cocktail also displayed similar cell numbers throughout the early culture (figure 1(f)), showing expansion was mainly achieved in the initial 48 h. Furthermore, morphological changes also occurred in all spheroid samples during the mitotic expansion phase (day 0 to 2). A significant proportion of the cells migrated and condensed from a homogeneous distribution across the hydrogel sphere into a dense spherical-like aggregate within the hydrogel sphere (D02 panels of figure 1(c)). These condensed aggregates had average diameters of 270 ± 50 μm ($N = 96$) as measured by manually fitting circular regions of interest to images acquired by a high content imager (ImageJ software, figure 1(e)). These images indicated that within an individual spheroid the cells had migrated from a dense homogeneous distribution across the sphere into an aggregate, with fewer cells located in the sphere than on day 0. It was found that cellular condensation was most pronounced in cell-repellent coated U-bottom well plates, hence these were selected for all subsequent culture. It was hypothesised greater cellular condensation would lead to more cell-to-cell contacts in the spheroid, resulting in more physiological tissue characteristics later in differentiation.

3T3-L1 spheroid characteristics during adipogenesis

In order to follow differentiation, spheroids were cultured up to 30 d to study cell morphology and adipose biology (figure 1(c)). Three different spheroid models were studied: singlets and triplets cultured with AC, and control triplets cultured without adipogenic cocktail (figure 1(c)). To differentiate spheroids into an adipose lineage, spheroids were exposed to the AC for 96 h (day 2 to 6) after the initial cell proliferation (day 0 to 2). Upon induction of adipogenesis, samples were then maintained in medium containing insulin (maintenance medium) to encourage lipogenesis (day 6 to day 30). As the spheroids differentiated, they became opaque across the entire structure in comparison to the initial time point and a small proportion of samples became buoyant by day 16 of culture (figure S5). The population of buoyant samples increased to 58% by day 29 of culture in one instance of singlets in a 96-well plate. These observations are indicative of ongoing lipogenesis with increases in intracellular lipid production leading to larger cells and a spheroid with an overall density lower than water. For both singlets and triplets, it was noticed that the cellular aggregate that condensed within the hydrogel sphere during expansion could become dislodged out of the hydrogel sphere (figure 1(C), day 16 singlet). These dislodged cellular aggregates still developed and grew in volume external to the hydrogel sphere. Cellular aggregates (both those encapsulated

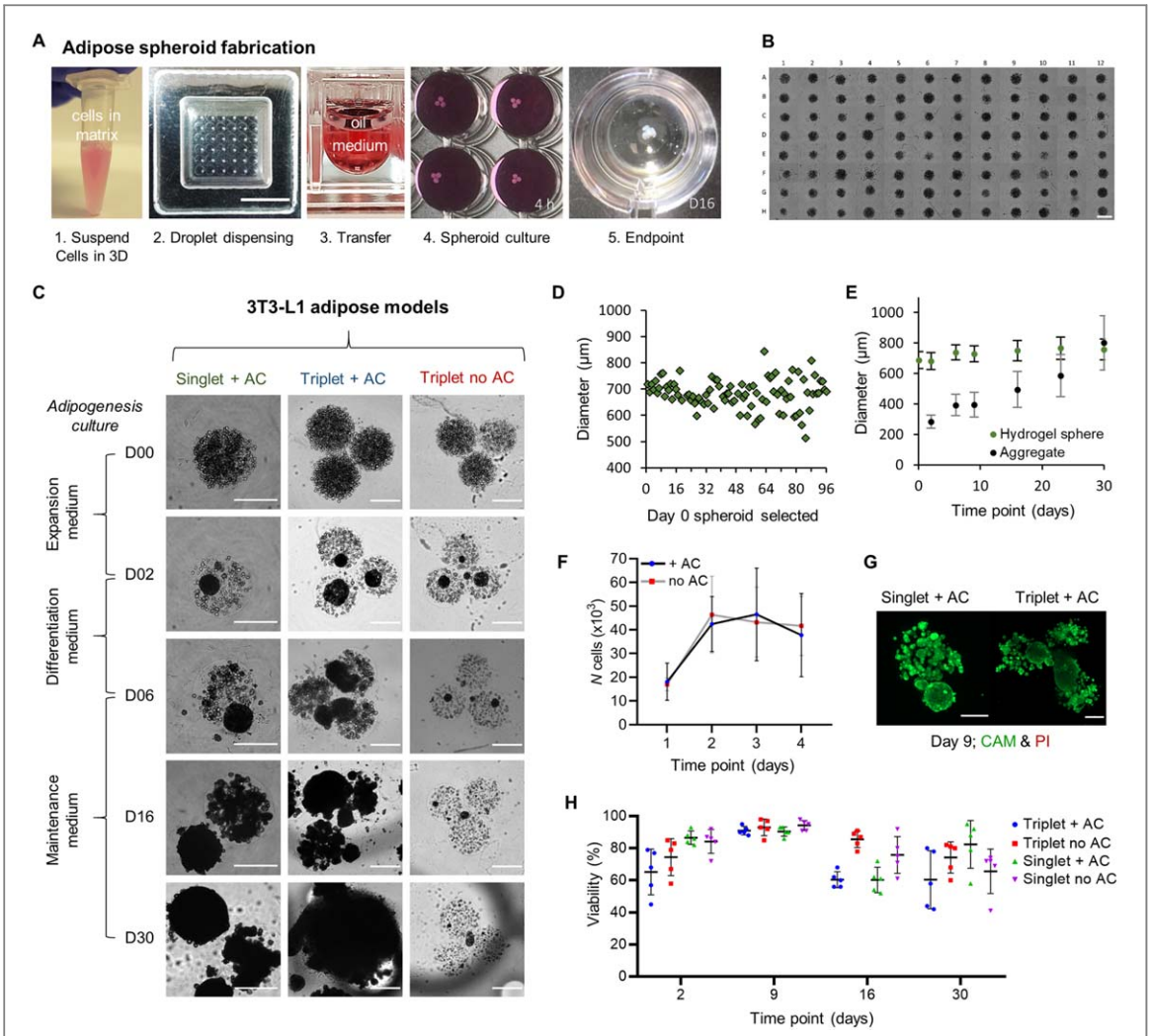

Figure 1. Fabrication and adipogenesis of 3T3-L1 spheroids in 96-well plates. (A) Photographs of the main steps of adipose spheroid fabrication: (A1) Suspension of cells into the 3D matrix at 40×10^6 ml^{-1}. (A2) Pipette dispensing of cellularised matrix as droplets into lipid-in-oil solution held within custom containers that have an array of 6×6 wells; each well contains one droplet which appear white in the photograph (1 cm scale bar). (A3) Transfer of solidified cellular droplets into wells containing oil above culture medium. (A4) Culture of cellular droplets (day 0 spheroids) after they sank into the medium phase. (A5) Endpoint analysis of differentiated spheroids. (B) An image matrix of brightfield micrographs of spheroids (day 0) within a 96-well plate. Scale bar 1 cm. (C) The development process for 3T3-L1 adipose models. Brightfield micrographs depict the development of singlet and triplet spheroids exposed to adipogenic cocktail (AC) and triplet spheroids with no AC exposure (control). Scale bar 500 μm. (D) Diameters of spheroids (day 0, 96-well plate) as determined by automated size analysis (Gen5 software). (E) Spheroid and aggregate diameters during culture (day 0 to 30, $N = 48$). (F) Cell numbers in early-stage spheroids cultured with and without AC as determined from an alamarBlue proliferation assay ($N = 5$ per condition). (G) Fluorescence micrographs of singlet and triplet spheroids stained for live cells (calcein-AM (CAM); green) and dead cells (propidium iodide (PI); red). Scale bar 250 μm. (H) Cell viabilities of adipose models (singlet and triplet $\pm$ AC exposure, $N = 5$ per condition) during culture as determined by image analysis software using fluorescence micrograph acquired by a high content imager.

within the sphere and those dislodged) grew in size up to 800 ± 180 μm diameter by day 30 for singlet spheroids. In some cases, the dislodged cellular aggregates grew to >1 mm in diameter, exceeding the size of their hydrogel sphere (figures 1(e) and S3). Furthermore, cellular rearrangement in the form of fusion of the spheroids, and their aggregates, was found for triplet samples cultured to day 30. Conversely, spheroids cultured without the adipogenic cocktail showed no or minor morphological changes after day 6 of culture. However, a decrease in the total number of cells in the 3D matrix was occasionally observed if samples were cultured to day 30. This morphological development of spheroidal cells during culture was highly reproducible with consistent behaviours occurring across the entire plate for the initial 16 d (figure S5).

The viability of cells within singlet and triplet spheroid ($N = 5$ per condition) was also investigated, by measurement of fluorescent signal from labelled cells (Gen5 software, figure S6). On day 2, viability was observed to be between 70% to 90% (figures 1(g) and (h)) and increased to >90% by day 9 regardless of the culture method. This demonstrated that the hydrogel-based matrix was not detrimental to 3T3-L1 cell viability. Beyond day 9, further growth of the cells in differentiating samples, caused cell viability to decline to ~60% on day 16 and 30, with the dead signal present at

the centre of the spheroid (figure S6). Compared to this, spheroids not exposed to AC remained highly viable on day 16 (~90%) but show a slight decrease in viability by day 30 (~70%). While 2D controls, show high viability (>95%) for the first 7 d of adipogenesis, after which the viability dropped to ~85% by day 14 (figure S7). This indicates that the adipogenesis cocktail is not toxic, but in long term culture the development of lipid-rich cells forms fragile monolayers which may trap dead cells and decrease viability. The cell death in differentiated spheroid samples was speculated to have arisen from an increase in the number and density of lipid-rich cells, leading to low nutrient availability and potential hypoxic conditions at the core of the spheroids. Hypoxia at the core would explain the dead signal that was located at the centre of spheroids (figure S6). As the peripheral cells showed high viability in this initial model, it was concluded that there would be sufficient healthy cells in 3D to study adipose characteristics.

Characterising the adipose biology of differentiating spheroids

We set out to characterise the adipose biology of 3T3-L1 cells in a 3D environment. Experiments were performed in comparison to a standard 2D model, to provide validation and assess the functional effects of growth in 3D. Specifically, the lipid phenotype and a targeted set of adipose-associated metabolites, adipokines and genes were characterised. All 2D cell controls were grown with an equivalent number of cells as compared to singlet spheroids i.e. 6000 cells per well (of a 96-well plate), unless otherwise stated. These control samples were allowed to proliferate for 72 h to reach confluency instead of the 48 h expansion that was applied to spheroids. Spheroids were treated as confluent in 3D after cellular condensation during the initial 48 h. This is based on the cells concentrating within the hydrogel as an aggregate and presumably forming cell-to-cell contacts. Thus, confluency was reached in 3D faster than in 2D.

Lipid morphology analysis

The development of lipid droplets within adipose spheroids and 2D controls was characterised by fluorescence microscopy on day 0, 7, 14 and 28 of adipogenic cocktail exposure (figures 2(a)–(c), and S8). Here, cells were labelled for lipid droplets (BODIPY 493/503), nuclei (Hoechst 33342) and the cell membrane (MemBrite^{TM}). Visualisation of the lipid stores across the periphery of one-half of a spheroid was possible and 3D image projections were created (figure 2(a) and movie S1). Specifically, spheroids ($N = 4$) were mounted for light sheet fluorescence microscopy (LSFM) by embedding in a hydrogel supporting structure and were imaged top down (figure 2(a)). Finer details of the lipid morphology in peripheral spheroid cells ($N = 4$, figures S8) and 2D control cells ($N = 3$, figure S9) were also captured by high magnification confocal fluorescence microscopy (CFM, figures 2(a)–(c)).

Using these approaches, it was observed that for all samples there were no lipid stores present at the start of adipogenesis, i.e. day 0 of AC. This was also supported by the amount of lipid signal relative to nuclei signal, as quantified by analysis of images acquire by a high-content imager ($N = 8$ spheroids and $N = 3$ 2D controls per time point, figure 2(d)). By day 7 of AC exposure, lipogenesis was induced as indicated by a low amount of lipid signal across segregated sections of the spheroid and 2D cells. Here, the relative lipid signal was higher in 2D samples than spheroids, indicating a slower initial development of lipid stores in a 3D environment. At day 14 of AC, lipid stores were present across both the spheroid and 2D samples, with the relative lipid signals reaching 80% $\pm$ 10% and 92% $\pm$ 4% respectively. Although the relative lipid signal was slightly lower for spheroid samples, the maximum width of the lipid droplets were slightly larger in spheroids at 25 $\pm$ 4 μm compared with 21 $\pm$ 3 μm for 2D (figure 2(e)). Indicating that the 3D cells maybe developing towards a more unilocular-like state. Microscopy also revealed the expression of lipid droplet-associated protein, perilipin 1 (PLIN) in adipose spheroids cultured to day 7 of AC or longer. PLIN, is required for efficient lipid droplet growth and promotes unilocular droplet formation [37], and should therefore be present in adipogenic tissue. As expected, PLIN was observed to be present around the edge of all intracellular lipid droplets in all differentiating samples (figure S10).

Extending the experiment duration, by allowing spheroids to differentiate for four weeks (28 d of AC) resulted in significant changes to cellular morphology. A notable change was the appearance of a large number of non-differentiated cells at the spheroid periphery, while lipid-containing cells were still found deeper into the spheroid (figure 2(a), panel D28 of AC). This was initially identified based on the lower relative lipid signal for day 28 spheroids in comparison to 2D samples, a value determined from images of the peripheral cells in spheroids. To better understand the lipid morphology at this stage, histology on spheroids was performed. While this method is commonly used on biopsies of WATs, lipid droplet features cannot be measured directly using this method though as the lipid is dissolved in the solvents applied during tissue processing. Thus, droplet sizes have to be quantified indirectly by measuring the size of the cavity where the lipid organelle was. In our experiments, lipid droplets were estimated to be $\geqslant$25 μm in diameter, and were observed towards the core of the sample in microtome sections (figures 2(f) and (g)). However, this method underestimates the actual lipid volume within the spheroid, particularly as the samples was found to shrink during the dehydration stage of tissue

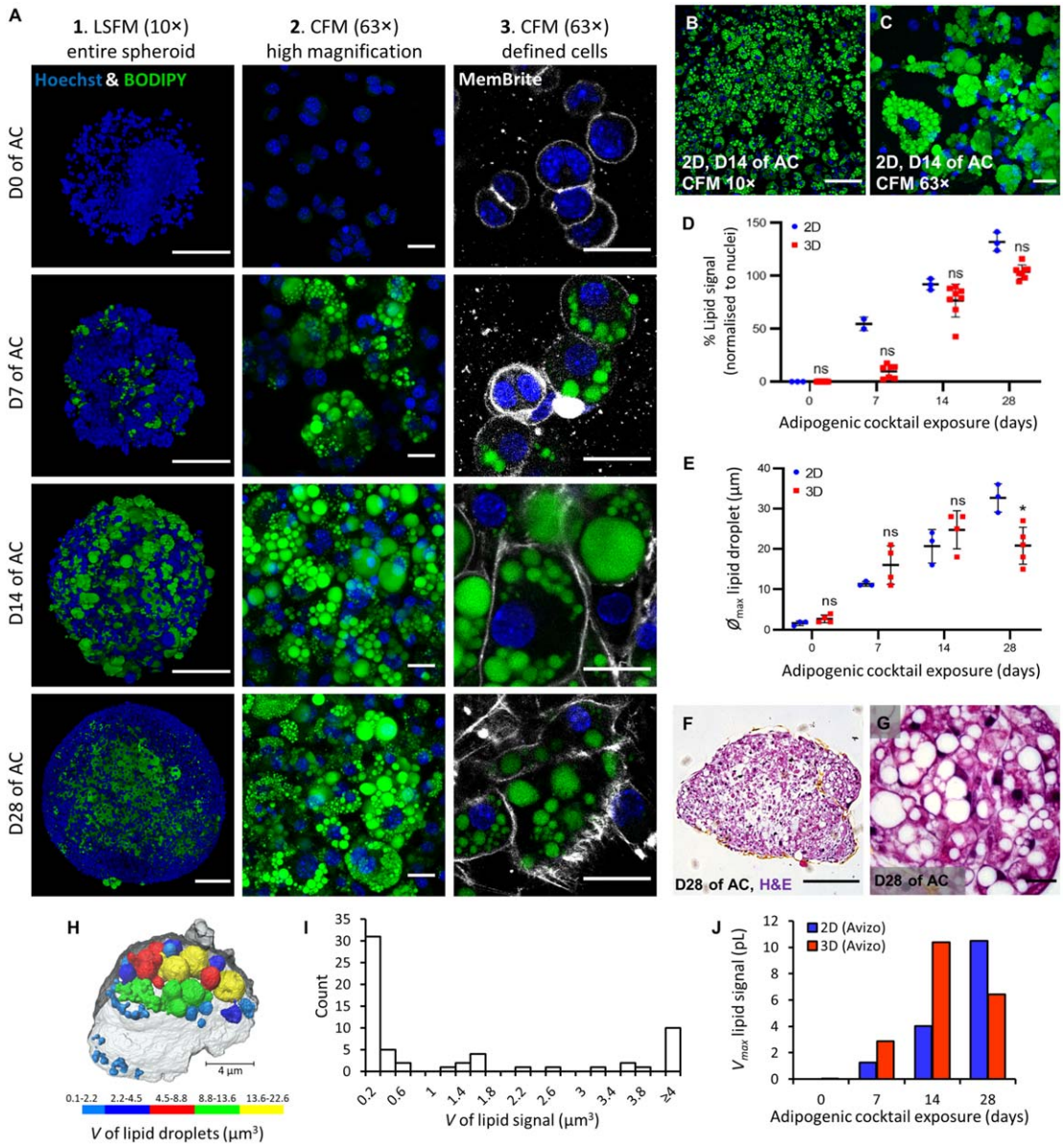

Figure 2. Lipid morphology of 3T3-L1 spheroids exposed to adipogenic cocktail. (A) A matrix of image projections depicting the change of lipid morphology within singlet spheroids over 28 d of adipogenic cocktail (AC) exposure. Spheroids were stained for nuclei (Hoechst 33342, blue), lipid droplets (BODIPY 493/503, green) and the cell membrane (MemBrite^{TM}, white). Fluorescence *z*-stack micrographs were acquired by either light sheet fluorescence microscopy (LSFM, (A1), 200 μm scale bar) or confocal fluorescence microscopy (CFM, (A2) and (A3), 25 μm scale bars). (B) and (C) Fluorescence micrographs of 2D controls (day 14 of AC) stained for nuclei and lipid droplets. Scale bars are 250 and 25 μm respectively. (D) Lipid fluorescence signal normalised to nuclei fluorescence signal in spheroids (denoted as 3D, $N = 8$) and 2D controls ($N = 3$) during culture. (E) Maximal diameter of a lipid droplet within 3D and 2D samples during culture ($N = 3$ per condition). (F) and (G) Colour micrographs of formalin-fixed paraffin embedded singlet spheroid (day 28 of AC). The spheroid was microtome sectioned (3 μm thick) and H&E stained. Scale bars are 250 and 25 μm respectively. (H)–(J) Proof of concept Amira-Avizo image analysis study. (H) An image of a 3D model of a single spheroidal cell containing lipid droplets segmented by their volume. (I) Histogram of the volume distribution of lipid droplets in model (H). (J) Maximal volume of lipid droplets within 2D and 3D models ($N = 1$). Significance was determined at specific time points between 2D and triplet spheroids with $^{*}P < 0.05$.

processing. These characteristics suggests cellular reorganisation occurred between day 14 and 28 of AC.

As *in vivo* adipose tissue has unilocular lipid stores while 2D typically favour multilocular lipid droplets, we wanted to assess the distribution of lipid droplets within spheroids and thus the extent of physiological similarity in an automated fashion. To date, limited methodologies have been developed to characterise the distribution of lipid droplet in maturing adipocytes. Of those reported, they are restricted to analysing images of adipose tissue or adipocytes, making 2D measurements of the lipid droplets within isolated cells, with the analysis performed in a manual or semi-automated fashion [38, 39]. Imaging provides a means of characterising the lipid phenotype and can be automated (along with the analysis) by applying the appropriate instrumentation and software. As such, we decided to assess the lipid morphology by

employing image-processing software Amira-Avizo (Thermo Fisher Scientific) to analyse our CFM imaging data (figures 2(a) and (c). Specifically, quantifying the volume and distribution of intracellular lipid droplets in spheroids by applying a protocol designed by 3Dmagination. For this proof of concept analysis, images that exhibited effective sample staining and were high-quality acquisitions in terms of focus, resolution and signal-to-noise ratio were selected and analysed ($N = 1$ per condition) with an aim to resolve the lipid droplet organelles. Initial results showed Amira-Avizo could identify the boundary of individual cells by recognizing the signal corresponding to the membrane. Furthermore, intracellular lipid droplets within the boundary were segmented by volume and the data for the distribution of these different volumes was produced as a histogram (figures 2(h) and (i)). The largest volume lipid droplets were also identified for each sample (figure 2(j)) and were measured as 10.4 pL (3D, day 14 of AC) and 10.5 pL (2D, day 28 of AC), a similar trend to those measured manually for lipid droplet diameter (figure 2(e)).

Targeted adipose-associated metabolites and adipokines

Release of metabolites and adipokines are associated with lipid metabolism in adipose tissue. Whilst the interpretation of the relative levels of individual metabolite and adipokines is challenging, their presence is a crucial requirement for a robust adipogenic model.

In our experiments metabolites and adipokines were measured for 2D and spheroid samples exposed to an adipogenic cocktail over 0, 3, 7, 10 and 14 d (figure 3, $N = 5$ samples per condition, in an identical volume of culture medium). To ensure accurate recordings were performed on spheroids they were co-cultured in triplicate to allow sufficient secretion of metabolite. It was observed that 2D cultures had limited utility when studying lipid metabolism for greater than 14 d as they lost cells with time. During differentiation, the 2D cells were observed to dissociate from the culture dish surface as cells increased their lipid storage. Consequently, the required number of cells in the 2D cultures for comparison to spheroids was not sufficient beyond 14 d of culture.

Glycerol and FFAs are the product of lipolysis of triglycerides within adipocytes, which are then secreted into the culture medium. Triglycerides are not normally exported from adipocytes, although some exosomal secretion of triglycerides has recently been reported [40]. As a measure of lipolysis we recorded the levels of glycerol and FFAs from medium conditioned 48 h prior to each point of the time course (figure 3(a)). Here, conditioned media refers to media exchanged for fresh solution prior to incubation. The levels of released metabolites in 2D control samples (6000 cells) were normalised to an equivalent number of cells as the triplet spheroids (~18 000 cells, supplementary discussion). In addition, background levels of the metabolites in the culture medium were subtracted from the measured values. Adipogenic cocktail exposure in both the 2D and spheroid samples resulted in increased levels of glycerol in the culture medium, compared with control samples, where release of these metabolites stayed <10 μmol (figure S11). The level of metabolites released in the case of spheroids was significantly lower than for 2D controls. Secreted glycerol levels for the spheroids showed a significant increase from day 7 of exposure to AC and maintained an increasing trend until day 14 exposure. This is in contrast to the, 2D model's glycerol levels which exhibited a slightly different trend, with glycerol levels significantly increasing at day 3 and 7 exposure and plateauing thereafter (figure 3(a)). Notably, this effect was not particularly correlated with cell viability at day 3 and 7 (100% and 95% respectively). This is indicative of triglyceride synthesis from glucose and subsequent lipolysis. Interestingly, later in differentiation, the released 2D levels of glycerol were observed to be ~13 times higher than in 3D. The significantly lower metabolite concentrations for spheroid samples raises the possibility that cell-to-cell contact and cell confluency in 3D resulted in more lipogenesis than lipolysis. The levels of FFAs were very low in both 2D and 3D cell culture, around the lower detectable limit for the assay. Although, in response to exposure to AC, FFAs were taken up from the media (below the levels found in fresh medium), supporting that there is active lipogenesis in both systems (figure 3(a)).

We then studied the release of hormones from the adipose models. Including, adiponectin which is associated with increasing basal glucose uptake and inhibiting lipolysis [41] and leptin, an adipocyte hormone that centrally supresses food intake and is associated with regulating fat stores. As with previous experiments, we measured the levels of these secreted adipokines from both 2D and 3D cells (figures 3(b) and S12). In our studies, secretion of adiponectin and leptin protein was only significant from the differentiating samples with hormone concentrations remaining low (<0.1 ng ml^{-1}) in non-differentiated spheroid samples (figures 3(b) and S12). For both 2D and spheroid samples, adiponectin linearly increased from day 7 to 14 of adipogenic cocktail exposure, with final concentrations of 13 ± 3 and 2.1 ± 0.5 ng ml^{-1} ($N = 5$, 2D normalised) respectively. In comparison, leptin secretion was more delayed during differentiation and was only observable from day 10 or day 14 of adipogenic cocktail exposure for the 2D (following a sigmoid pattern) and spheroid samples respectively. However, likewise with the glycerol assay, leptin and adiponectin secretion were significantly lower in spheroids than 2D, specifically, 14 fold and 6 fold respectively.

The lower 3D adipokine results raised the question of whether the spheroid matrix could trap proteins

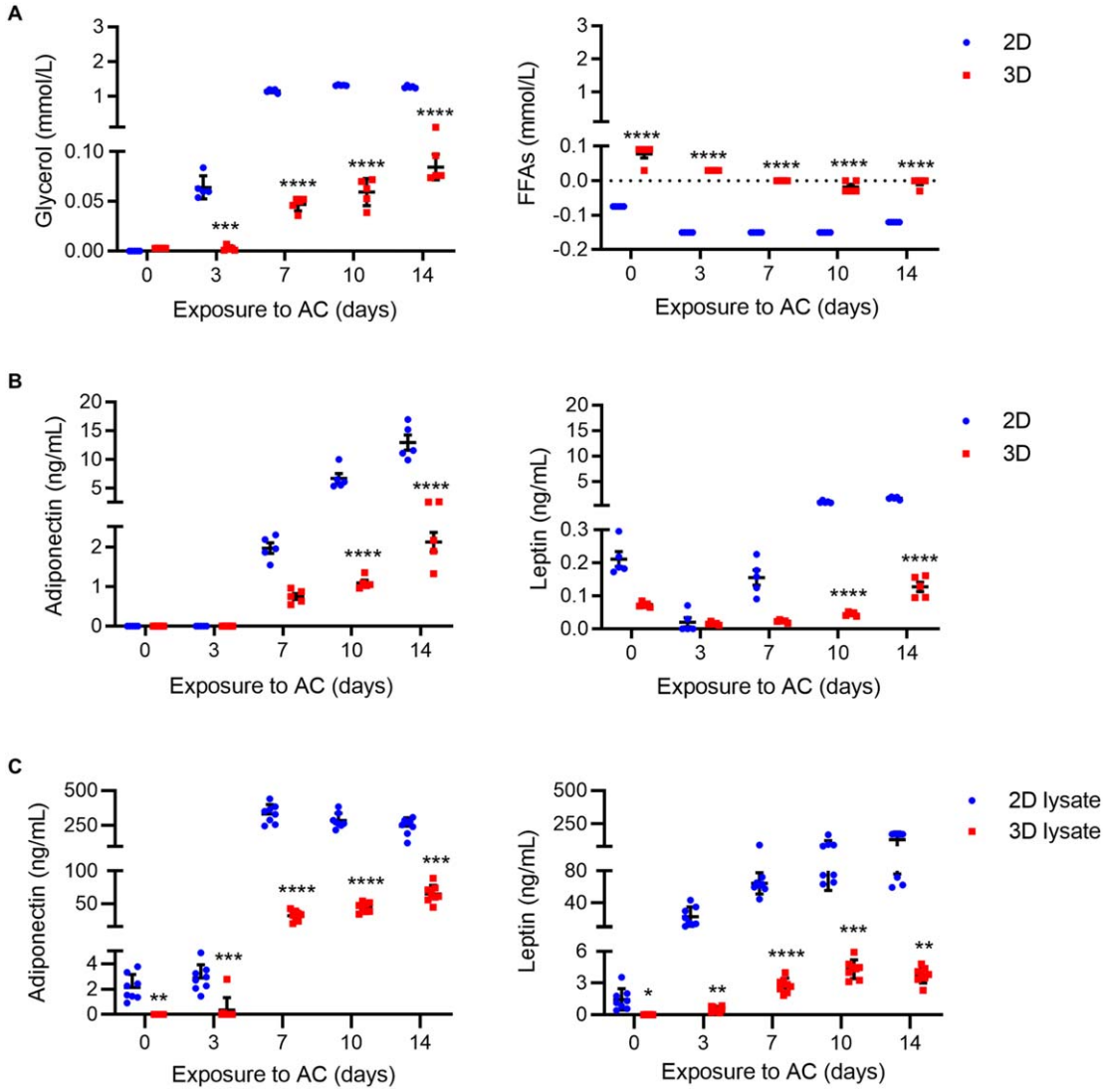

Figure 3. Targeted metabolic and adipokine behaviour of 2D cells and spheroids during adipogenesis. (A) Time course concentrations of glycerol and free fatty acids (FFA) in the culture media of 2D and triplet spheroid models ($N = 5$ per condition). (B) and (C) Time course concentrations of adiponectin and leptin in: (B) the culture medium of 2D and triplet spheroid models ($N = 5$ per condition) and; (C) the lysate of 2D and triplet spheroid models ($N = 8$ per condition). The time course was 0, 3, 7, 10 and 14 d of AC exposure, with the culture media conditioned for 48 h before all measurements. The 2D readings were multiplied three-times to match with triplet spheroids (2D models contained 6000 cells/well initially, while each spheroids encapsulated ~6000 cells initially, (see supplementary discussion). Spheroids were denoted as 3D in the graph legend. Significance was determined at specific time points between: 2D and triplet spheroids using supernatant (A and B) and 2D and spheroid lysate (C) with $^{*}P < 0.05$, $^{**}P < 0.01$, $^{***}P < 0.001$ and $^{****}P < 0.0001$.

such as adipokines, and that this could be a reason for lower levels of secretion into the culture medium. In order to address this question, spheroids were lysed and analysed for levels of adiponectin and leptin (figure 3(c)). Strikingly, the levels of both hormones in the lysate were significantly higher than in spheroid culture supernatant and higher or comparable to 2D supernatant respectively. Therefore, adipocyte derived hormones are either trapped in the spheroid matrix or are not secreted.

Adipose-marker gene expression

The extent of adipogenesis observed at the gene expression level was measured using a panel of eight genes, in 2D and spheroids. These genes are ascribed with important roles at different stages of differentiation inclusive of initiation transcription factors (*Pparγ* and *Cebpα*), glucose uptake (*Glut*4), lipid transport and metabolism (*Fabp*4, *Fasn* and *Lipe*), lipid storage and regulation (*Plin*1) and adipokines (*Adipoq*).

We used droplet digital PCR (ddPCR) to quantitate differential gene expression at the RNA level. *Canx* was used as housekeeping gene based on a geNorm kit for mouse applied to select the least variable gene during adipogenesis. The gene of interest and housekeeping gene were labelled with FAM and VIC respectively and used within each of these droplet reactors. We investigated the expression of these genes

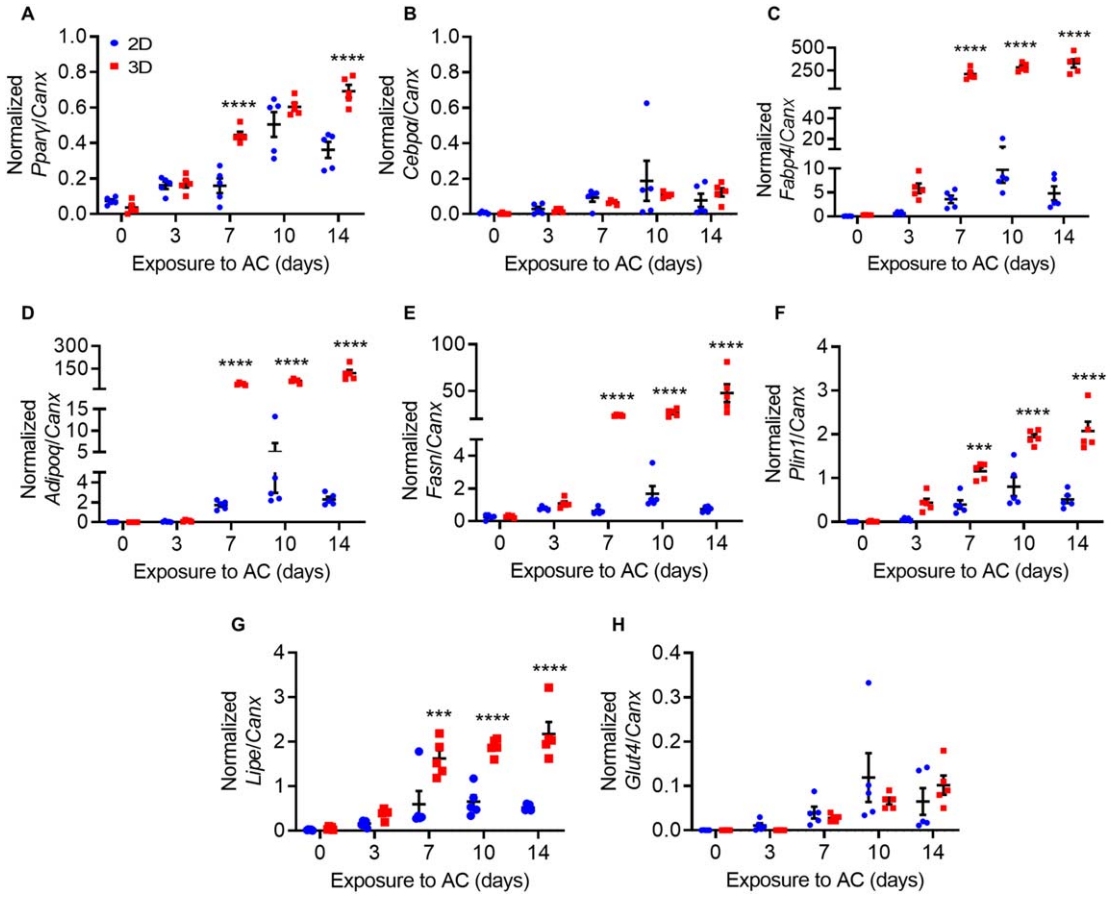

Figure 4. Adipose marker gene expression in 2D cells and spheroids during adipogenesis. (A)–(H) Time course gene expression profile of adipose differentiation markers in 2D and triplet spheroid models ($N = 5$ per condition): (A) *Pparγ*; (B) *Cebpα*; (C) *Fabp4*; (D) *Adipoq*; (E) *Fasn*; (F) *Plin1*; (G) *Lipe*; and (H) *Glut4*. All gene expression levels were determined by ddPCR, with each gene normalised to *Canx*. The time course was 0, 3, 7, 10 and 14 d of AC exposure. Spheroids are denoted as 3D on the graphs. Significance was determined between differentiated 2D and triplet spheroids at specific time-points with $^{***}P < 0.001$ and $^{****}P < 0.0001$.

at five time points of exposure to adipogenic cocktail (day 0, 3, 7, 10 and 14) with $N = 5$ biological replicates for each experimental condition (figure 4).

Both the 2D and spheroid models showed increased expression of adipose markers in differentiated samples compared to non-differentiated ones (figures S13(a)–(h) and S14(a)–(h)). For example, *Pparγ* shows increased expression from day 3 onwards in 2D and spheroids relative to day 0 (figures S13(a) and S14(a)). The 2D cells did not show significant upregulation for *Cebpα* (transcription factor) but 3D spheroids displayed significant increased expression from day 7 onwards relative to non-differentiated controls (figures S13(b) and S14(b)). While the expression level of *Adipoq* (adiponectin) showed a large divergence between 2D and spheroids. In the 2D model, *Adipoq* show significant expression relative to non-differentiated controls on day 10 onwards, whereas for spheroids there is significant expression day 7 onwards (figures S13(d) and S14(d)). We also observed significantly higher expression of *Plin1* in spheroids compared with 2D models correlating with lipid droplet formation. It is interesting to observe that 3D spheroids showed significant expression of *Plin1* relative to non-differentiated controls at day 3 onwards whereas in 2D it happened at day 7 (figures S13(f) and S14(f)).

In the comparison between day 14 spheroids and 2D cultures we observed strikingly higher expression of genes with lower variance in spheroids (figures 4(a)–(h)). Specifically, the expression was significantly higher in spheroids for the genes *Pparγ* (2 fold), *Fabp4* (40 fold), *Adipoq* (50 fold), *Fasn* (40 fold), *Plin1* (4 fold) and *Lipe* (4 fold) suggesting an enhanced degree of differentiation in spheroids (figures 4(a), (c)–(g)). While, *Cebpα and Glut4* showed similar expression levels in both culture systems (figures 4(b) and (h).

In order to further evaluate the degree of differentiation in spheroids we then compared relative gene expression in mature subcutaneous mouse adipose tissue with 2D and 3D cells at 14 d of differentiation (figure S15). Strikingly *Fabp4* and *AdipoQ* were expressed at much higher levels in 3D spheroids than *in vivo* tissue. This could reflect the heterogeneity of adipose tissue compared to a pure adipocyte cell culture and/or that the 3D cultures are developing in a way consistent with mature tissue. The level of *Fasn* was similar between 3D and *in vivo* tissue. These data suggest that 3D adipose spheroids are, in terms of gene

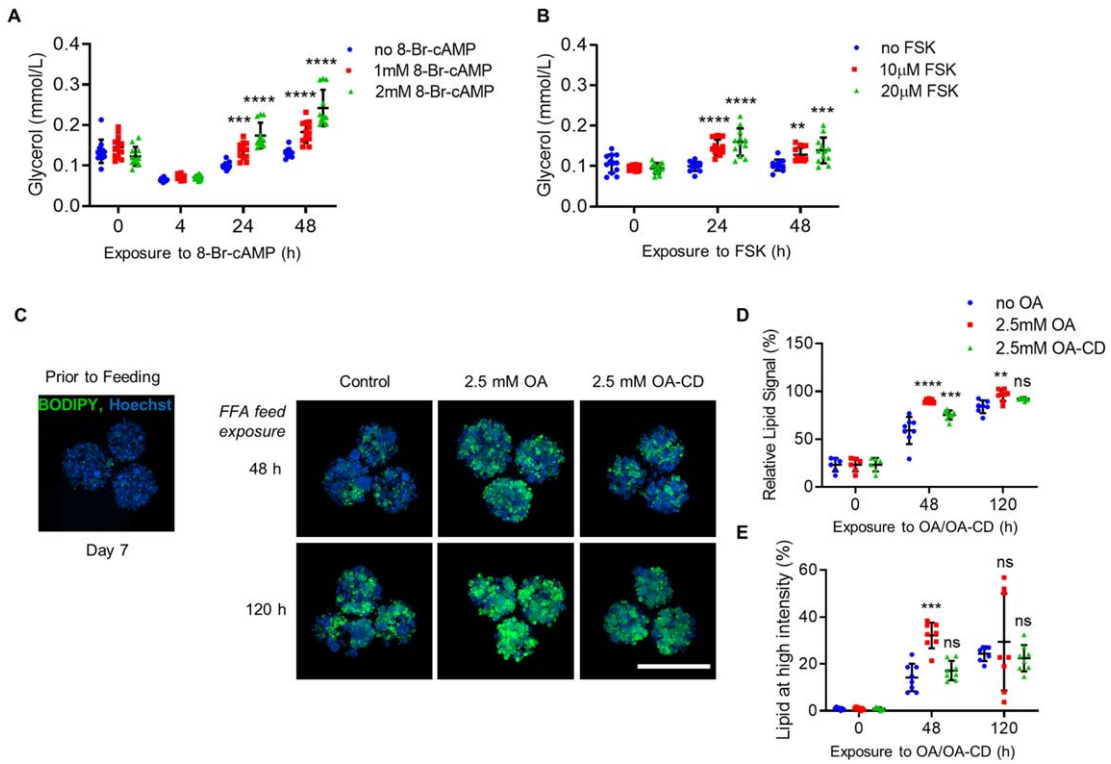

Figure 5. Modulation of lipid metabolism in 3D WAT model. (A) and (B) Time course concentrations of glycerol in the culture medium of day 12 spheroids (triplets, $N = 12$ per condition) on induction of lipolysis by exposure to either (A) 8-Br-cAMP (at 0, 1 and 2 mM) or (B) forskolin (FSK, at 0, 10 and 20 μM) both in the absence of insulin. The culture medium was conditioned prior to each measurement for: (A) 24, 4, 20 and 24 h for each time point respectively and; (B) 24 h for all time points. (C) Images of spheroids during the time course of a free fatty acid (FFA) feeding. Day 7 spheroids ($N = 8$ per condition) were cultured with either unconjugated oleic acid (OA), cyclodextrin conjugated-OA (OA-CD) or without OA (control). Spheroids were stained for nuclei (Hoechst 33342, blue) and lipid droplets (BODIPY 493/503, green). Scale bar 1 cm. (D) Relative lipid signal (i.e. lipid signal normalised to nuclei signal as a percentage) in spheroid samples described in (C). (E) High-intensity lipid signal (i.e. signal with greater than 15,000 intensity per pixel) in spheroid samples described in (C). Significance was determined between treated and untreated spheroids at each time point with $^{**}P < 0.01$, $^{***}P < 0.001$ and $^{****}P < 0.0001$.

expression, at least expressing key genes at similar or higher levels to mature tissue, in contrast to 2D cultures.

Our experiments established that the adipogenic 3T3-L1 spheroids showed a range of complex functions: lipid storage, metabolite generation, adipose marker expression and could therefore be a suitable adipose model for biomolecular testing.

Metabolic and phenotypic response of adipose spheroids to biomolecules

We next investigated whether the 3T3-L1 spheroids could be used as a model system for probing WAT function and response. Such a model should be reactive to the variation of external cues, such as nutrients, hormones and/or drugs. With the anticipated response being a change in the viability, lipid morphology or lipid metabolism of the adipocytes.

Modelling lipolysis in the 3D WAT model

First, we explored whether reagents could modulate the behaviour of lipid metabolism in the adipose spheroids i.e. the 3D WAT model, specifically by increasing lipolysis. In lipolysis, hormone-sensitive lipase (HSL) catalyses the hydrolysis of triglyceride to release FFAs and glycerol. Adipocytes generally express low levels of glycerol kinase and therefore glycerol recycling is normally low, thereby measurement of glycerol provides an estimate of the level of lipolysis [42, 43].

Firstly, we used 8-Br-cyclic adenosine monophosphate (8-Br-cAMP), a cAMP analogue as a second messenger trigger for triglyceride lipolysis by HSL. Adipose spheroids cultured to day 12 were selected for treatment as these had adequate stores of lipids to monitor induced lipolysis. Two doses of 8-Br-cAMP (1 and 2 mM) were selected from published 2D studies. Exposure of adipose spheroids to 8-Br-cAMP resulted in a dose-dependent response increasing the concentration of glycerol in the medium after 24 and 48 h compared to untreated spheroids, with the spheroid response to the 2 mM dose higher than the 1 mM dose (figure 5(a)). The increased glycerol levels indicate enhanced break-down of triglyceride in response to levels of 8-Br-cAMP within the spheroid's adipocytes. The metabolic response was not discernible at 4 h exposure although the medium was only conditioned for 4 h as opposed to 24, 20 and 24 h for the 0, 24 and 48 h time points respectively (figure 5(a)).

Secondly, we then repeated the experiment using forskolin, a cell-permeable diterpenoid activator of adenylyl cyclase, known to increase intracellular levels of cAMP. The experiment was designed in order to activate lipolysis, through a more physiologically relevant activation of the pathway. The concentration of glycerol was increased, in a dose dependent way, in the 24 h conditioned culture medium supernatant at 24 and 48 h of forskolin exposure (10 and 20 μM) relative to untreated spheroids (figure 5(b)). Interestingly, levels were found to be lower at 48 h compared to 24 h, although still significantly higher than in untreated spheroids suggesting that there may be some modulation of the cAMP signal.

Hence lipolysis, could be triggered in a dose-dependent manner in adipose spheroids using two different treatments.

Modelling storage and lipogenesis in the 3D WAT model

Next, we considered whether the introduction of fatty acids could promote lipid storage and triglyceride synthesis in adipose spheroids. Oleic acid (OA), a naturally occurring fatty acid, was fed to early stage, i.e. day 7, adipose spheroids when lipogenic gene expression was activated (figures 4 and 5(c)). OA was used both in its unconjugated form (ethanol solubilised) or conjugated to cyclodextrin (CD, water solubilised). To monitor the increase of lipid content within spheroids during OA feeding, samples were fluorescently labelled for lipid droplets (BODIPY 493/503) and nuclei (Hoechst 33342, figure 5(c)) at different time points during the feeding study. Automated measurements of the area of the fluorescent signals were performed by image analysis (Gen5) on high content images (figure S4). This allowed an output of relative lipid signal (i.e. lipid signal normalised to nuclei signal) to account for the variance in the number of cells within spheroids. Using this method, it was shown that the relative lipid signal within early stage adipose spheroids at day 7 increased significantly during the 48 h feeding of 2.5 mM OA or 2.5 mM OA-CD relative to the control (figure 5(d)). Compared to spheroids cultured without OA the relative lipid signal increased by 52% and 27% respectively. The lower effectiveness of OA-CD at increasing the lipid signal in spheroids suggests that although OA is less soluble, it was better at entering the 3D cells and being converted into lipid stores, potentially as it is less sterically restricted.

Extending the feeding duration from 48 to 120 h resulted in a low magnitude increase in lipid content for spheroids fed with OA and OA-CD, with only the OA-fed samples showing a significant increase relative to unfed controls. This was a result of the unfed spheroids showing a significant increase in their lipid content at 48 and 120 h relative to the 0 h time point (two-way ANOVA, P-value $= 0.0001$).

Furthermore, the feeding of spheroids with OA over 48 h resulted in a significant proportion of the recorded lipid signal being at high-intensity relative to culturing spheroids without OA (figure 5(e)), indicative of these regions having a high concentration of lipophilic dye, hypothesised to be the result of high lipid concentrations. Here, high-intensity was defined as signal greater than 15,000 intensity per pixel, signal intensity may be recorded up to a maximum value of 65,536 per pixel (16-bit CCD camera). We also observed a similar but non-significant trend of increased high-intensity lipid signal in spheroids were fed with OA-CD for 48 h. However, when extending feeding to 120 h, we did not find any significant increase of high-intensity lipid signal for spheroids fed either OA or OA-CD relative to unfed spheroids. For OA-fed spheroids, there is a large distribution of the proportion of high-intensity lipid signal on day 5 of feeding. We speculate that this is a consequence of the applied standardised image protocol not being appropriate for samples showing buoyant properties. At least two of the OA-fed spheroids were at higher vertical positions and were imaged out of focus with lower intensity fluorescence signal recorded. Hence, the quantification of relative lipid signal by automated counting of the fluorescent signal intensity, in its current form, may not be as informative for highly differentiated samples which have attained high-concentrations of lipid and have become partially buoyant. Thus, without further analysis of the internal lipid content it is difficult to determine whether more lipids are being stored in the feeding samples over this medium-term growth (of 120 h). However, we have shown that lipid storage was increased in early-stage (i.e. day 7) adipose spheroids by feeding with fatty acids.

High-throughput drug response screening in the 3D WAT model

Finally, we investigated whether the 3D adipose model was responsive to drug treatment, with an aim to screen compounds in a high-throughput manner. For this study we chose rosiglitazone, a thiazolidinedione agonist of PPARγ, as a known activator of adipogenesis (see for example [10]).

Specifically, we monitored an entire 96-well plate of triplet spheroids cultured with rosiglitazone over a time course for glycerol released into the culture medium (on day 2, 6 and 9) and performed endpoint characterisation of spheroids for their lipid phenotype and viability (day 9, figure 6(a)). We worked on a 96-well scale which enabled high-throughput characterisation of the lipid phenotype and cell viability by image acquisition (of spheroids labelled for lipids and nuclei) using a high content fluorescence imager. For the lipid phenotype assay, as in the previous experiments, the acquired 96-well images were analysed for the sum area of both lipid and nuclei signal (figure 6(b)). While

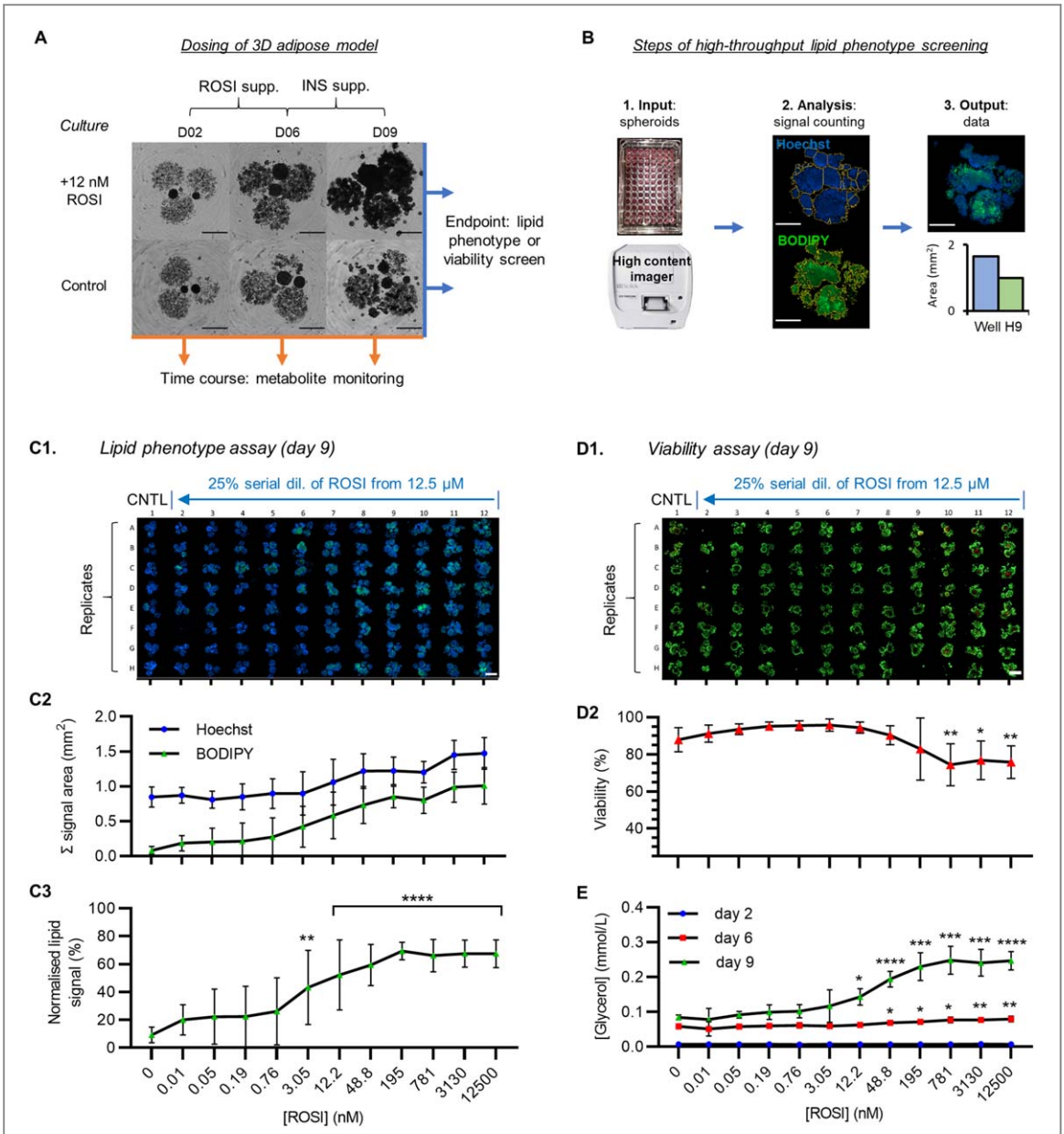

Figure 6. High-throughput drug dose-response of the 3D adipose model. (A) Outline for rosiglitazone (ROSI) drug and insulin (INS) supplement dosing of triplet adipose spheroids (3D adipose model). Brightfield micrographs depict the triplet spheroids during culture. 500 μm scale bar. (B) Outline for lipid phenotype screening with application of a high-content imager (Cytation 1, BioTek) and image analysis software. Here, the output were image sets and signal area count data. (C)–(E) Rosiglitazone dosing of the 3D adipose model (96-well scale), assessed by: (C) lipid phenotype assay (day 9), (D) viability assay (day 9) and (E) glycerol secretion monitoring (day 2, 6 and 9). Dosing was between day 2 to 6, applying a serial dilution of rosiglitazone from 12.5 μM (column 12) to 11.9 pM (column 2), with column 1 left as an non-dosed control (CNTL). (C1). Image matrix of the entire plate of spheroids stained for nuclei (Hoechst 33342, blue) and lipid droplets (BODIPY 493/503, green). Scale bar 1 cm. (C2). Graph of the sum area of nuclei and lipid droplet signals. (C3). Graph of the lipid signal normalised to nuclei signal. (D1). Image matrix of the entire plate of spheroids stained for live cells (calcein-AM, green) and dead cells (propidium iodide, red). Scale bar 1 cm. (D2). Graph of spheroid viabilities. (E) Graph of glycerol concentration in culture medium. Each graph displays data from $N = 8$ spheroid replicates per dose. Significance was determined at specific time points in response to rosiglitazone dosage with $^{*}P < 0.05$, $^{**}P < 0.01$, $^{***}P < 0.001$ and $^{****}P < 0.0001$.

for the viability assay, the sum area of both live cells and dead cells was determined.

Preliminary tests were performed to determine the approximate potency of the drug. Exposure to 3T3-L1 spheroids from day 2 to 6 showed responses to as low as 1 nM concentration. Using this as a benchmark concentration, adipose spheroids were exposed to a 25% serial dilution of rosiglitazone from 12.5 μM to 12 pM across an entire 96-well plate, with $N = 8$ replicates per concentration (figure 6(c1)). Endpoint characterisation revealed an increase in lipid and nuclei signal area with increasing dose from 1 nM exposure (figure 6(c2)). Normalisation of the lipid signal (relative to nuclei signal) revealed a dose response curve (figure 6(c3)). Specifically, a sigmoidal trend of increasing normalised lipid signal with increasing rosiglitazone dose, with a significant difference in lipid signal observed for the 48.8 nM dose and higher doses

compared with the undosed control. A similar trend was observed for 2D controls (figure s16), with normalised lipid signal levels comparable to 3D for all doses except 3.05 and 12.2 nM where spheroid lipid signal was significantly higher.

The viability assay revealed the drug was not toxic to spheroids on day 6, with the average spheroid viability >85% for all rosiglitazone concentrations (figure s17). While on day 9, a significant drop in viability (to ∼75%) was observed for dose 781 nM and higher (figure 6(d)). This is likely attributed to the spheroids accumulating more lipid, reducing the extent of nutrient penetration to the core cells of the spheroids and in turn decreasing viability. Similar trends were observed in day 16 adipose spheroids (figure 1(e)), indicating rosiglitazone has increased the rate of differentiation of spheroidal cells.

Rosiglitazone affected the viability of 2D control cells similarly (figure s18), with viability declining at the final time point to ∼55% average for the higher doses (781 and 3130 nM). Interestingly, the 2D viability increased to 78% ± 18% average for the highest dose (12500 nM), potentially the proportion of dead cells did increase but were more prone to dissociation and were not visible in the assay, this would account for the large spread.

Drug responsive behaviour was also revealed by the time course monitoring of the glycerol concentration in 48 h conditioned culture medium supernatant (day 2, 6 and 9, figure 6(d)). Immediately before rosiglitazone exposure (day 2), all spheroids displayed the same base level of glycerol. At day 9, a sigmoidal treatment response was observed for levels of glycerol with rosiglitazone, a similar pattern to that of the lipid signal (figure 6(e)). This trend was also matched in 2D controls (figure s16), except as was observed in non-dosed adipogenic samples, secreted metabolite concentrations were lower in spheroids than in 2D controls.

These data show that spheroids have a dose-dependent response, in terms of lipid accumulation and glycerol secretion, to rosiglitazone.

Discussion

In this study we describe a 3D adipose model, comprising spheroids of 3T3-L1 cells efficiently differentiated into adipocytes. The adipose model was highly characterised for lipid morphology, glycerol secretion, and expression of selected adipokines and adipogenesis genes. The method for producing the spheroids is straight-forward and does not require the use of specialist equipment and cell number can be scaled via the use of groups of spheroids.

Developing and automating a reproducible adipose spheroid model

This model was both robust in terms of reproducibility, with low variance in both the fabrication process (9% CV of droplet diameter) and the spheroid differentiation process (in terms of spheroid morphology and adipogenesis characteristics). The work presented here was by manual production, which while accessible to most laboratories, is labour intensive and costly in terms of time. However, by employing 96-well plates we enabled high-throughput workflows such as liquid handler-based processing (for culture and assays) and high content imaging (for characterisation). The next step is development of automation for the fabrication processes, increasing throughput, improving size-control and potentially reducing variance. This is feasible, as the matrix employed and the fabrication workflows are compatible with a variety dispensing techniques including pipetting, drop-on-demand bioprinting [30] and syringe pump driven microfluidics, all of which are amenable to automation. An automated workflow will improve experimental reproducibly and repeatability in the future. Prototypes of syringe-pump based dispensing robots built by OxSyBio Ltd have demonstrated that spheroid dispensing can be reduced to 5 min per 96-well plate, with size variance reduced to ∼5% CV (unpublished work). Further, precision generation of smaller spheroids, down to 300 μm, would also significantly reduce or eliminate dead cell presence at the core of spheroids which was observed in spheroids by day 16.

However, one consideration when maintaining differentiating adipose spheroids from day 16 onwards is spheroid buoyancy following lipid accumulation. Handling the spheroids became challenging, as the probability of spheroid buoyancy and their subsequent loss in liquid handling steps increased. This risk may be reduced by altering the culturing methodology, and by restricting the movement of the spheroid to prevent floating. Residual oil has also been noticed at the media interface of samples at late stages of culture. While this contaminant appears not to be detrimental to spheroid culture, the oil can lead to background signals during the lipid phenotype assay. As such, the oil was manually removed by pipetting prior to labelling dye addition, decreasing the overall throughput. In the future, this oil may potentially be removed with a volatile solvent wash step or by adding further oil solvent to the top of the well to dilute the background signal.

The simplicity of our workflow has high potential for an automated high-throughput screening system which would be a prerequisite for its use in drug screening. Kingelhutz *et al* have adapted their scaffold-free hanging drop adipose spheroid system to a 384 well ultra-low attachment (non-inverted) plate for high-throughput screening [13]. Their system is limited to a single spheroid per well, whereas our use of a matrix in the spheroid manufacture process, allows control of spheroid size together with the potential for multiple spheroids within one well and therefore an increase of target cell number. The use of a matrix also

allows customisation of the supporting scaffold, which can be tailored to promote adipogenesis and the phenotypes of interest. We envisage future 3D adipose models may incorporate additional components from the extracellular matrix of adipose tissues and multiple cell types to promote tissue development in a manner similar to those seen organoid systems [35]. The vascularized adipose system described by Muller *et al* forms spheroids in ultra-low attachment plates and then selected spheroids are incorporated into Matrigel. This is a multistep 3D-culture process and less adaptable to high-throughput screening than our system, which forms spheroids directly in the screening plate [16]. Some of the other biofabrication approaches offer more complexity but are currently low throughput and are difficult to upscale to high-throughput screening platforms [18, 44]. Bioreactor and microfluidics systems are exciting alternative 3D models but are similarly less amenable to lost-cost high throughput drug screening approaches [23, 25, 45].

A highly differentiated adipose spheroid model

We demonstrated that mature adipose cells have formed by day 14 of adipogenesis, with the 3D cells showing high signal for lipid stores and upregulation of adipogenic genes and adipokines. Studied in conjunction with 2D models (which revealed similar trends), the 3D model displayed larger lipid droplets (up to 28 μm diameter) and the upregulation (up to 50-fold) of multiple genes critical in adipogenesis. Encouragingly, gene expression in 3D samples was similar or higher to *in vivo* tissue, consistent with a highly differentiating model system. Although 2D models secreted higher levels of adipokines (up to 10 fold), we also found that lysates of spheroids had ~30 times higher adipokine levels than in their culture medium, raising the possibility of protein trapping in the spheroid matrix or of regulated reduced secretion. The sigmoidal pattern of leptin secretion, at least in 2D cultures, could reflect the chronic insulin treatment, possibly leading to a steady state maximal response, given that acute exposure is reported to increase leptin secretion particularly under treatment conditions that include a PPARg agonist in the differentiation medium [46]. Future modifications to the structure and the matrix as well as introducing vasculature may address the former issue. The level of glycerol secretion was also higher in 2D cultured cells although this could reflect stronger and possibly more physiological suppression of lipolysis by insulin in the 3D model.

Crucially, the 3D adipose model could also be cultured for 4-weeks at which point they became buoyant as lipid stores further developed. Here, cellular reorganisation was observed, with a population of non-differentiated cells present at the surface of the spheroid whilst lipid containing cells were found deeper into the structure. The origin of these cells is unclear although previous studies have demonstrated that adipose cells, such as those found in mammary or dermal depots are capable of dedifferentiation (see for example [47, 48]). Our current hypotheses are that the undifferentiated cells present within the spheroid undergo further proliferation over time and migrate into the space around the core of differentiated cells, or that they may also arise through a process of dedifferentiation. It would be interesting to investigate whether these cells could be induced to undergo further differentiation. The potential to retain a population of cells capable of undergoing further differentiation could be valuable in studies of adipose hyperplasia. Compared to 2D, the 3D model was also more mechanically robust as 2D models easily dissociated from their culture plates on prolonged culture and were easily damaged during mounting onto coverslips.

A functionally responsive adipose spheroid model

We have shown that the 3D model had an active lipid metabolism which could be modulated and easily monitored by released metabolites, adipokines and their lipid phenotype. Hence lipolysis, a key function of adipose tissue hydrolysing triglycerides and secreting FFA and glycerol to meet metabolic demand in other tissues, could be significantly increased in a dose-dependent manner in adipose spheroids using the cAMP analogue 8-br-cAMP or forskolin to activate adenylyl cyclase and thus upregulate cellular cAMP levels. Further, lipid storage was promoted by feeding the cells oleic-acid in the presence of insulin. These data set the foundation for using the 3D adipose model to screen the effects of adipose-active drugs.

A drug responsive adipose spheroid model

As a proof of concept for drug responsiveness, we exposed spheroids to rosiglitazone, a PPARγ activating drug. Treatment of type 2 diabetes patients with rosiglitazone is reported to suppress peripheral adipocyte lipolysis by increasing their insulin sensitivity [49]. However, in human primary adipocytes *in vitro,* rosiglitazone in the presence of insulin increased both hormone sensitive lipase (HSL) and lipoprotein lipase (LPL) expression, suggesting that both lipolysis and lipogenesis were increased [50]. This is similar to our observations while using adipose spheroids, of dose dependent increased lipid stores and release of glycerol. In 3T3-L1 cells it has also been shown that rosiglitazone, in combination with insulin and high glucose, increased glycerol secretion and also reduced Oil Red O staining of lipid [51]. The secretion of glycerol is consistent with the direction of effect in our studies, but in contrast we also observed increased cellular lipid content. However, in that study mature adipocytes were treated, in contrast we carried out treatment during adipocyte differentiation, thus the differences in lipid accumulation may reflect the pro-adipogenic effect of rosiglitazone.

We have thus shown that adipose spheroids are drug responsive with dose-dependency using a variety of high throughput compatible end-point assessments. The 3D adipose model therefore has the potential for enabling the discovery of new adipose-modifying drugs by performing tests on novel drug candidates or compound-hit screening on currently approved drug libraries, which may be repurposed. This system could also be used for determining half maximal inhibitory concentration (IC_{50}) or half maximal effective concentration (EC_{50}) for adipose-targeting drugs. Future humanization of the model and addition of other cell types will further increase the utility of this model in drug screening.

Functional imaging of the adipose spheroid model

We showed the potential of high content imaging and the power of Amira-Avizo software for quantifying lipid morphology and lipid volume, which could be applied to high throughput screens using spheroids. Although, in order to ensure accurate segmental analysis, further improvements to the staining methodology and the reduction of signal scattering in the imaging is required to resolve the smallest lipid droplets. However, using methods such as this greatly improves the ability of researchers to extract quantitative information from multi-dimensional data reproducibly and quickly.

Another imaging challenge has been the characterisation of cells at the core of spheroids, which is a problem inherent in working with 3D cellular organisations/tissue models. Microscopic techniques, such as CFM, for the most part suffer from light penetration issues in biological tissues, with fluorescent signal acquisition limited to around 100–200 μm depths. While histology of spheroids requires cumbersome hydrogel-embedding techniques and results in shrunken samples with no lipid content. However, future studies applying highly penetrating imaging techniques such as multiple-photon microscopy at around 1300–1700 nm (the second biological and water window in imaging) may enable comparative studies between core and peripheral cells [52].

Conclusion

Our study has established a highly differentiated model with active lipid metabolism which can be modulated with small molecules. This system is a scalable 96-well 3D adipose model capable of efficient differentiation which is drug-responsive and as such may be used as a powerful tool to help inform preclinical and mechanistic studies. Spheroid handling processes may also be fully automated and high throughput with minor adjustments to workflows and the incorporation of robots for fabrication opening the high throughput studies. For example, screening for new adipose-targeting drugs using commercially available compound libraries. The model could be humanised by using primary human cells, adipose cell lines and potentially adipocytes from iPSC cells. In these experiments cells could be chosen with particular genotypes or edited using CRISPR/Cas9 technology to investigate the genetics, for example, of fat distribution. Finally, future models can also be adapted to further mimic *in vivo* adipose physiology by including vascular cells, macrophages and adipocytes sourced from primary or patient cells, opening the way for mechanistic studies in metabolic disease.

Acknowledgements

We thank various groups and individuals for their assistance during the project. The teams at OxSyBio Ltd: Biofabrication, Synthetic Biology, Engineering and Production, as well as the entire Cox lab for their feedback and advice on the research. The Clinical Chemistry team and ddPCR team at the Medical Research Council (MRC) Harwell Institute for characterising the metabolite levels and genetic expression respectively. The Central Laser Facility (CLF) at the Research Complex at Harwell for access to the OCTOPUS microscopy facility and 3Dmagination for image analysis using the Amira-Avizo software. Antoine Fouillet (BioTek) and Hayley Croswell (Integra Biosciences) for their assistance in setting up automated processes on instruments. The Science & Technology and Facilities Council staff involved in setting up OxSyBio's laboratory. Professor Hagan Bayley for his input and general discussions. Professor Wayne Hayes at the University of Reading for access to their Rheometer.

Funding

This work was co-funded between OxSyBio Ltd (venture capital) and the Cox lab of the MRC Harwell Institute (academic grants). The Cox lab was supported by Medical Research Council (UK) MC_U142661184 funding. The collaboration was also partly supported by grants awarded by the STFC: the Harwell HealthTec Cluster proof of concept proposal (2017 and 2018) and Bridging for Innovators (B4i, 2018).

Author contributions

ADG and RP lead the project while, JG, SNO and RDC oversaw the project. SWB, XX and LB contributed ideas to the project. ADG, RP, JG, SNO and RDC conceived the experiments. ADG and RP designed and performed the experiments. ADG fabricated all spheroids, while RP performed all 2D controls and cultured all fabricated samples. RP performed targeted adipose metabolite measurements, adipokines profiling, preparations

and analysis for ddPCR characterisation. AJA and LT performed the ddPCR experiments. AC acquired imaging data for spheroid samples using light-sheet fluorescence and confocal fluorescence microscopy. ADG performed all other microscopy and high-content imaging. KM analysed the imaging data sets using Amira-Avizo. TSB performed the rheological analysis of the hydrogel-based matrix. LAKZ performed mouse tissue biopsy and RNA isolation. VST cultured the cell line and performed the histology. ADG, RP and RDC wrote the paper with contributions from all authors.

Competing interests

The work described here was partly funded and supported by OxSyBio Ltd a small and medium enterprise (SME) commercial company aimed at creating therapeutic tissue using synthetic biology. ADG, VST, TB, XX, JG and SNO were directly employed by OxSyBio Ltd. In-kind support from OxSyBio Ltd was also given to the Cox group at MRC Harwell Institute in order to carry out the project.

Data and materials availability

Supplementary information is available in the online version of the paper.

ORCID iDs

Roger D Cox https://orcid.org/0000-0001-7170-5014

References

[1] Zheng Y, Ley S H and Hu F B 2018 Global aetiology and epidemiology of type 2 diabetes mellitus and its complications *Nat. Rev. Endocrinol.* **14** 88–98
[2] Vazquez G, Duval S, Jacobs D R Jr and Silventoinen K 2007 Comparison of body mass index, waist circumference, and waist/hip ratio in predicting incident diabetes: a meta-analysis *Epidemiol. Rev.* **29** 115–28
[3] Canoy D 2008 Distribution of body fat and risk of coronary heart disease in men and women *Curr. Opin. Cardiol.* **23** 591–8
[4] Wang Y F, Rimm E B, Stampfer M J, Willett W C and Hu F B 2005 Comparison of abdominal adiposity and overall obesity in predicting risk of type 2 diabetes among men *Am. J. Clin. Nutr.* **81** 555–63
[5] Roth G A *et al* 2017 Global, regional, and national burden of cardiovascular diseases for 10 causes, 1990 to 2015 *J. Am. Coll. Cardiol.* **70** 1–25
[6] Di Cesare M *et al* 2016 Trends in adult body-mass index in 200 countries from 1975 to 2014: a pooled analysis of 1698 population-based measurement studies with 19.2 million participants *Lancet* **387** 1377–96
[7] Pulit S L *et al* 2019 Meta-analysis of genome-wide association studies for body fat distribution in 694 649 individuals of European ancestry *Hum. Mol. Genet.* **28** 166–74
[8] Loos R J F 2018 The genetics of adiposity *Curr. Opin. Genet. Dev.* **50** 86–95
[9] Zeggini E, Gloyn A L, Barton A C and Wain L V 2019 Translational genomics and precision medicine: moving from the lab to the clinic *Science* **365** 1409–13
[10] Lefterova M I, Haakonsson A K, Lazar M A and Mandrup S 2014 PPARgamma and the global map of adipogenesis and beyond *Trends Endocrinol. Metab.* **25** 293–302
[11] Siersbaek R *et al* 2017 Dynamic rewiring of promoter-anchored chromatin loops during adipocyte differentiation *Mol. Cell* **66** e425
[12] Serrero G and Khoo J C 1982 An *in vitro* model to study adipose differentiation in serum-free medium *Anal. Biochem.* **120** 351–9
[13] Klingelhutz A J *et al* 2018 Scaffold-free generation of uniform adipose spheroids for metabolism research and drug discovery *Sci. Rep.* **8** 523
[14] Naderi N *et al* 2014 Adipogenic differentiation of adipose-derived stem cells in 3-dimensional spheroid cultures (microtissue): implications for the reconstructive surgeon *J. Plast. Reconstr. Aesthet Surg.* **67** 1726–34
[15] Turner P A, Gurumurthy B, Bailey J L, Elks C M and Janorkar A V 2017 Adipogenic differentiation of human adipose-derived stem cells grown as spheroids *Process Biochem.* **59** 312–20
[16] Muller S *et al* 2019 Human adipose stromal-vascular fraction self-organizes to form vascularized adipose tissue in 3D cultures *Sci. Rep.* **9** 7250
[17] Daquinag A C, Souza G R and Kolonin M G 2013 Adipose tissue engineering in three-dimensional levitation tissue culture system based on magnetic nanoparticles *Tissue Eng.* C **19** 336–44
[18] Sakai S, Ohi H, Hotta T, Kamei H and Taya M 2018 Differentiation potential of human adipose stem cells bioprinted with hyaluronic acid/gelatin-based bioink through microextrusion and visible light-initiated crosslinking *Biopolymers* **109** e23080
[19] Pati F *et al* 2014 Printing three-dimensional tissue analogues with decellularized extracellular matrix bioink *Nat. Commun.* **5** 3935
[20] Abbott R D *et al* 2016 The use of silk as a scaffold for mature, sustainable unilocular adipose 3D tissue engineered systems *Adv. Healthc. Mater.* **5** 1667–77
[21] Feng J *et al* 2017 An injectable non-cross-linked hyaluronic-acid gel containing therapeutic spheroids of human adipose-derived stem cells *Sci. Rep.* **7** 1548
[22] Hsiao A Y, Okitsu T, Teramae H and Takeuchi S 2016 3D tissue formation of unilocular adipocytes in hydrogel microfibers *Adv. Healthc. Mater.* **5** 548–56
[23] Gerlach J C *et al* 2012 Adipogenesis of human adipose-derived stem cells within three-dimensional hollow fiber-based bioreactors *Tissue Eng.* C **18** 54–61
[24] Ward A, Quinn K P, Bellas E, Georgakoudi I and Kaplan D L 2013 Noninvasive metabolic imaging of engineered 3D human adipose tissue in a perfusion bioreactor *PLoS One* **8** e55696
[25] Loskill P *et al* 2017 WAT-on-a-chip: a physiologically relevant microfluidic system incorporating white adipose tissue *Lab Chip* **17** 1645–54
[26] Kongsuphol P *et al* 2019 *In vitro* micro-physiological model of the inflamed human adipose tissue for immune-metabolic analysis in type II diabetes *Sci. Rep.* **9** 4887
[27] Feng J W *et al* 2017 An injectable non-cross-linked hyaluronic-acid gel containing therapeutic spheroids of human adipose-derived stem cells *Sci. Rep.* **7** 1548
[28] Kim Y, Baipaywad P, Jeong Y and Park H 2018 Incorporation of gelatin microparticles on the formation of adipose-derived stem cell spheroids *Int. J. Biol. Macromol.* **110** 472–8
[29] Silva K R *et al* 2016 Delivery of human adipose stem cells spheroids into lockyballs *PLoS One* **11**
[30] Graham A D *et al* 2017 High-resolution patterned cellular constructs by droplet-based 3D printing *Sci. Rep.* **7** 7004
[31] Ulrich T A, Jain A, Tanner K, MacKay J L and Kumar S 2010 Probing cellular mechanobiology in three-dimensional culture with collagen-agarose matrices *Biomaterials* **31** 1875–84
[32] Zhou M *et al* 2009 Self-assembled peptide-based hydrogels as scaffolds for anchorage-dependent cells *Biomaterials* **30** 2523–30

[33] Jokinen J et al 2004 Integrin-mediated cell adhesion to type I collagen fibrils J. Biol. Chem. 279 31956–63
[34] Semler E J, Ranucci C S and Moghe P V 2000 Mechanochemical manipulation of hepatocyte aggregation can selectively induce or repress liver-specific function Biotechnol. Bioeng. 69 359–69
[35] Takebe T and Wells J M 2019 Organoids by design Science 364 956–9
[36] Comley K and Fleck N A 2010 A micromechanical model for the Young's modulus of adipose tissue Int. J. Solids Struct. 47 2982–90
[37] Sztalryd C and Brasaemle D L 2017 The perilipin family of lipid droplet proteins: gatekeepers of intracellular lipolysis Biochim. Biophys. Acta, Mol. Cell. Biol. Lipids 1862 1221–32
[38] Boschi F, Rizzatti V, Zamboni M and Sbarbati A 2015 Models of lipid droplets growth and fission in adipocyte cells Exp. Cell. Res. 336 253–62
[39] Sun Z Q et al 2013 Perilipin1 promotes unilocular lipid droplet formation through the activation of Fsp27 in adipocytes Nat. Commun. 4 1594
[40] Flaherty S E et al 2019 A lipase-independent pathway of lipid release and immune modulation by adipocytes Science 363 989
[41] Fu Y C, Luo N L, Klein R L and Garvey W T 2005 Adiponectin promotes adipocyte differentiation, insulin sensitivity, and lipid accumulation J. Lipid Res. 46 1369–79
[42] Large V, Peroni O, Letexier D, Ray H and Beylot M 2004 Metabolism of lipids in human white adipocyte Diabetes Metab. 30 294–309
[43] Viswanadha S and Londos C 2008 Determination of lipolysis in isolated primary adipocytes Methods Mol. Biol. 456 299–306
[44] Hsiao A Y, Okitsu T, Teramae H and Takeuchi S 2016 3D tissue formation of unilocular adipocytes in hydrogel microfibers Adv. Healthc. Mater. 5 548–56
[45] Ward A, Quinn K P, Bellas E, Georgakoudi I and Kaplan D L 2013 Noninvasive metabolic imaging of engineered 3D human adipose tissue in a perfusion bioreactor PLoS One 8 e55696
[46] Zeigerer A, Rodeheffer M S, McGraw T E and Friedman J M 2008 Insulin regulates leptin secretion from 3T3-L1 adipocytes by a PI 3 kinase independent mechanism Exp. Cell. Res. 314 2249–56
[47] Zhang Z et al 2019 Dermal adipose tissue has high plasticity and undergoes reversible dedifferentiation in mice J. Clin. Invest. 129 5327–42
[48] Wang Q A et al 2018 Reversible de-differentiation of mature white adipocytes into preadipocyte-like precursors during lactation Cell. Metab. 28 e283
[49] Mayerson A B et al 2002 The effects of rosiglitazone on insulin sensitivity, lipolysis, and hepatic and skeletal muscle triglyceride content in patients with type 2 diabetes Diabetes 51 797–802
[50] McTernan P G et al 2002 Insulin and rosiglitazone regulation of lipolysis and lipogenesis in human adipose tissue in vitro Diabetes 51 1493–8
[51] Wang P et al 2007 Absence of an adipogenic effect of rosiglitazone on mature 3T3-L1 adipocytes: increase of lipid catabolism and reduction of adipokine expression Diabetologia 50 654–65
[52] Guesmi K et al 2018 Dual-color deep-tissue three-photon microscopy with a multiband infrared laser Light-Sci. Appl. 7 12